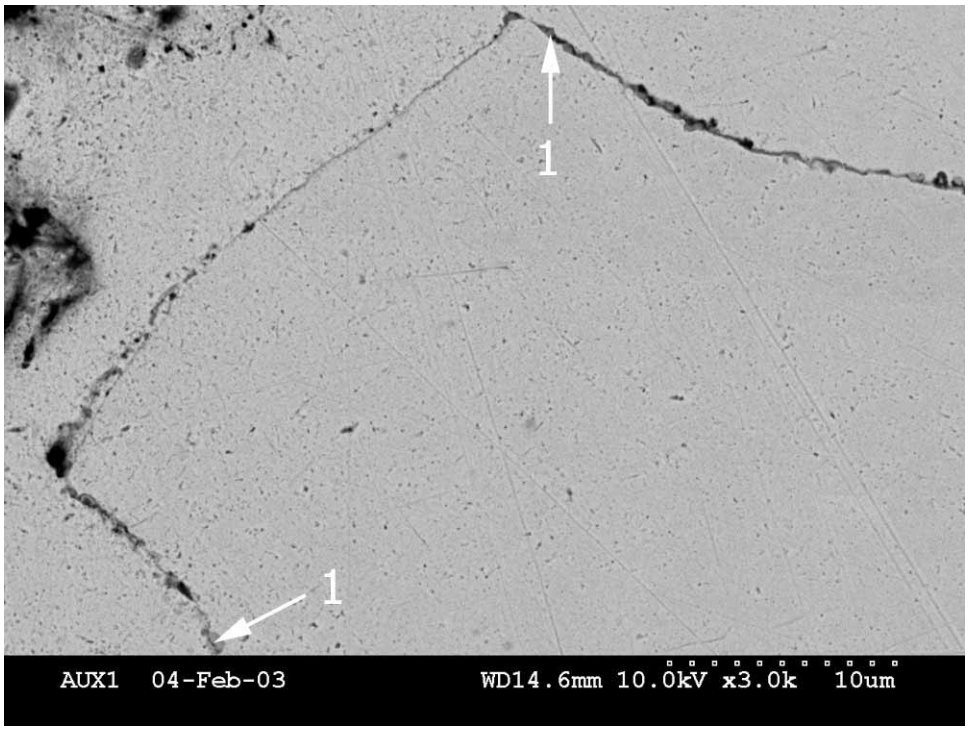

Reference micrograph for EDS results below

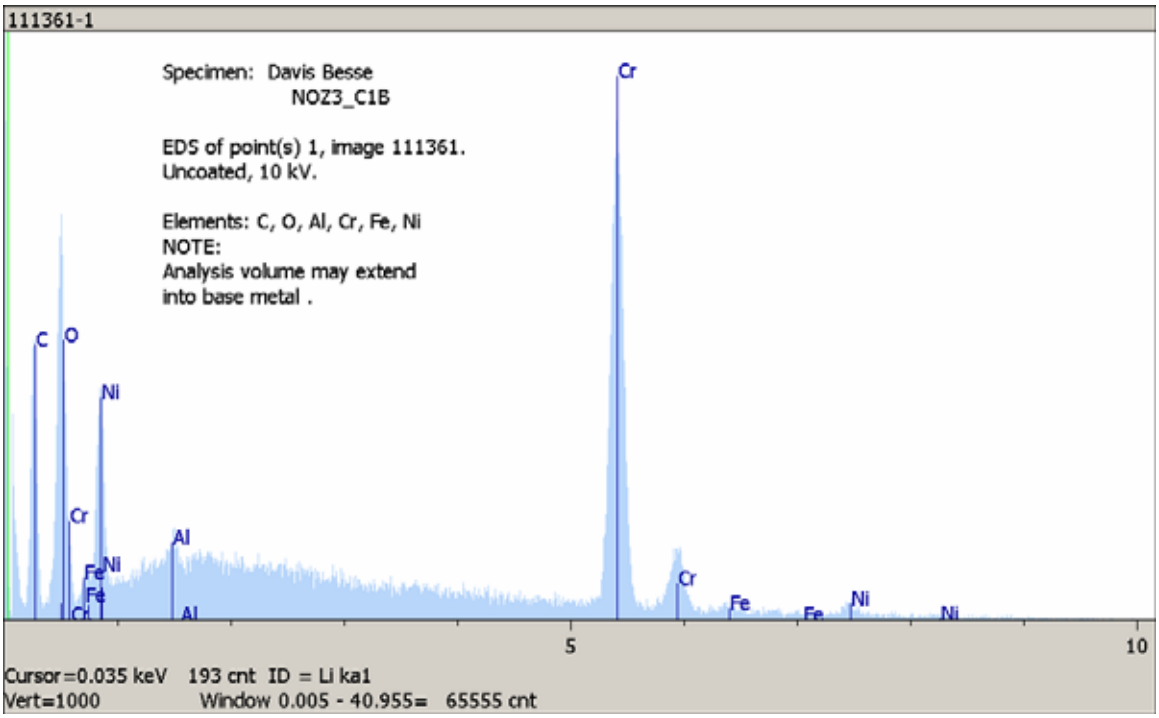

Figure 2.7.3: The grain boundary (points designated "1") contained carbon, oxygen, aluminum, chromium and nickel.

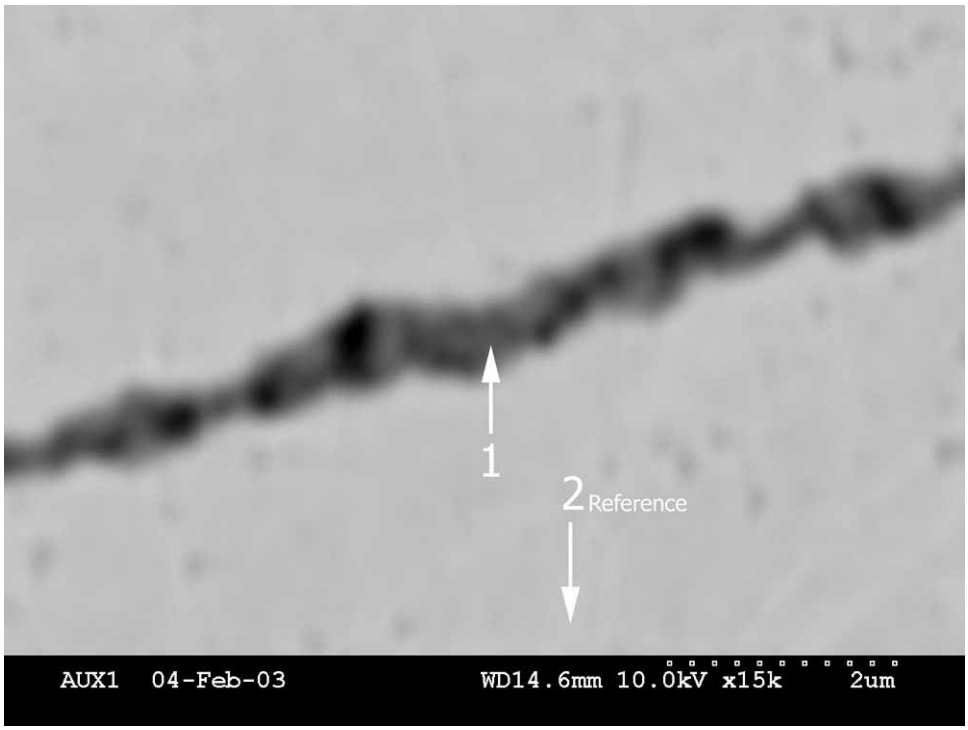

BSE 15,000X

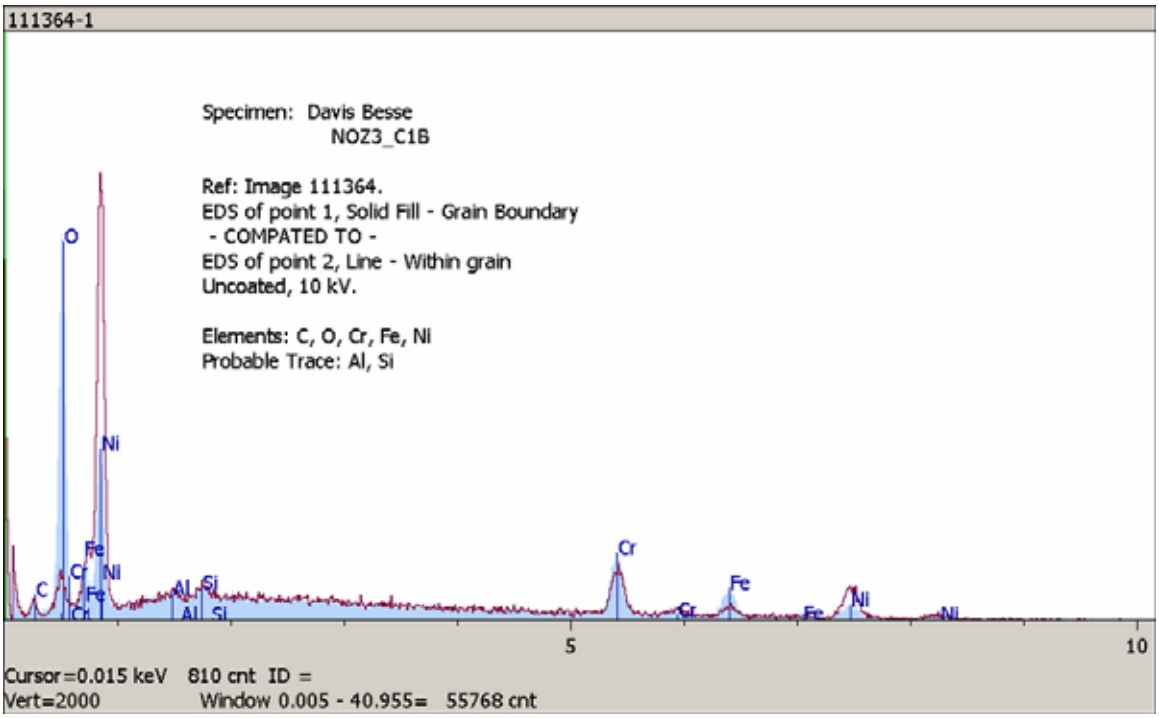

Figure 2.7.4: The grain boundary (solid fill) contained higher oxygen and chromium compared to the bulk grain (line spectrum) (Note: The BSE image was defocused in order to optimize the EDS count rate.)

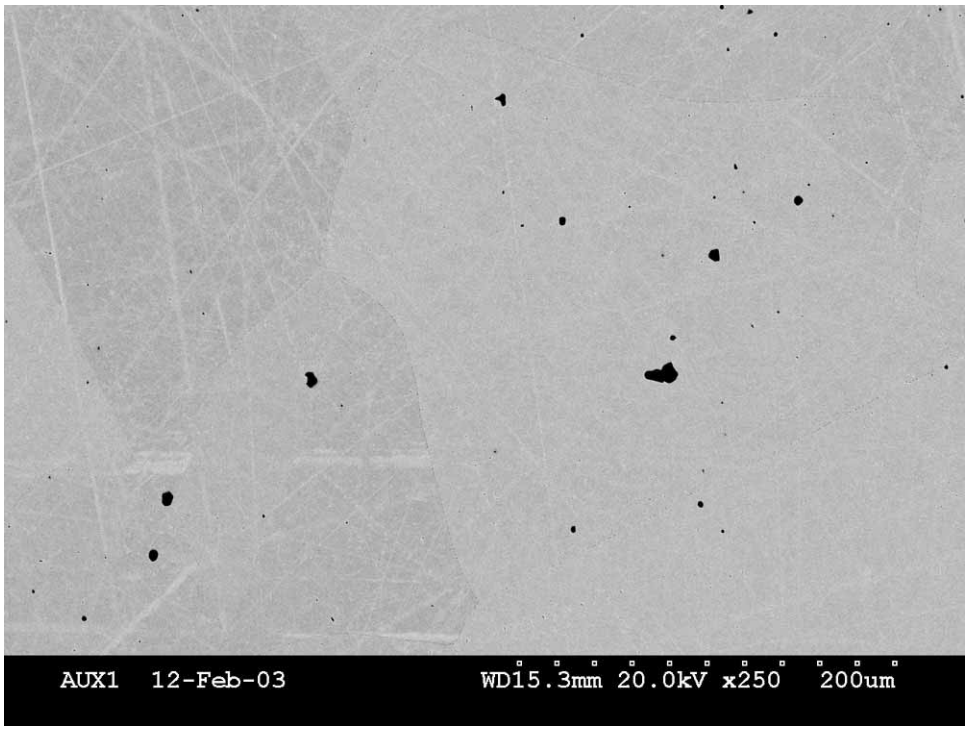

Reference micrograph for EDS semi-quantitative analysis

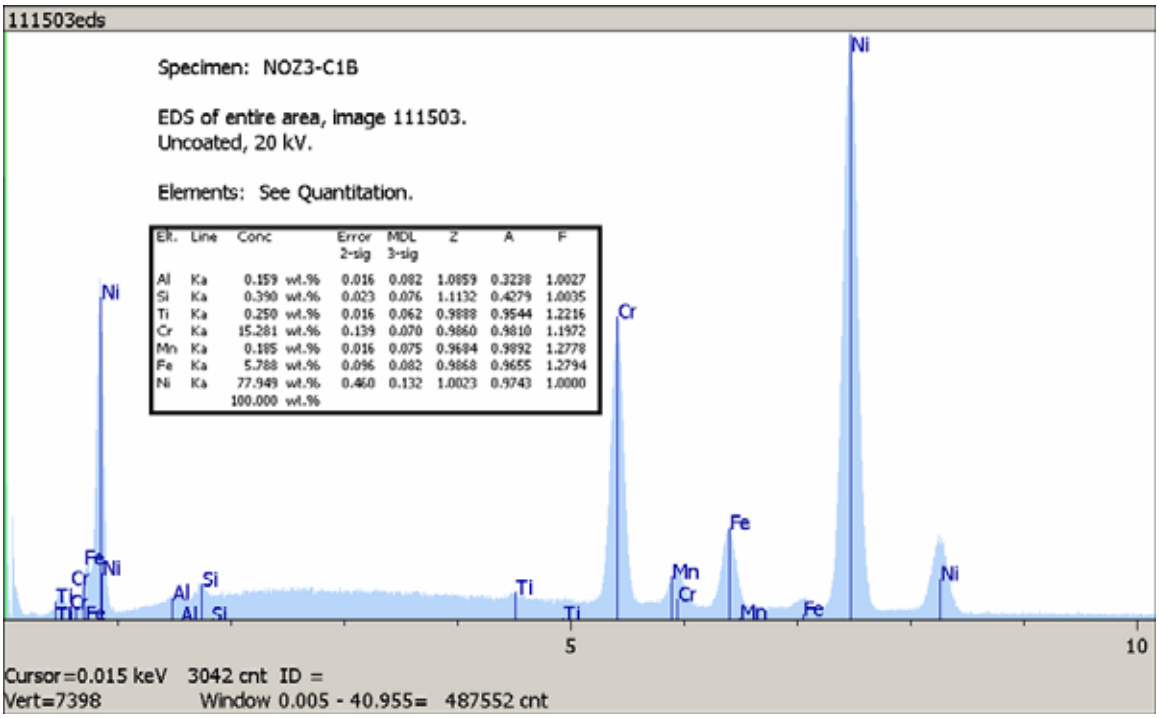

Elt.	Line	Conc		Error 2-sig	MDL 3-sig	Z	A	F
Al	Ka	0.159	wt.%	0.016	0.082	1.0859	0.3238	1.0027
Si	Ka	0.390	wt.%	0.023	0.076	1.1132	0.4279	1.0035
Ti	Ka	0.250	wt.%	0.016	0.062	0.9888	0.9544	1.2216
Cr	Ka	15.281	wt.%	0.139	0.070	0.9860	0.9810	1.1972
Mn	Ka	0.185	wt.%	0.016	0.075	0.9694	0.9892	1.2778
Fe	Ka	5.788	wt.%	0.096	0.082	0.9868	0.9655	1.2794
Ni	Ka	77.949	wt.%	0.460	0.132	1.0023	0.9743	1.0000
		100.000	wt.%					

Figure 2.7.5: Reference micrograph and semi-quantitative EDS results for nozzle material. The results appeared consistent with those expected for Alloy 600.

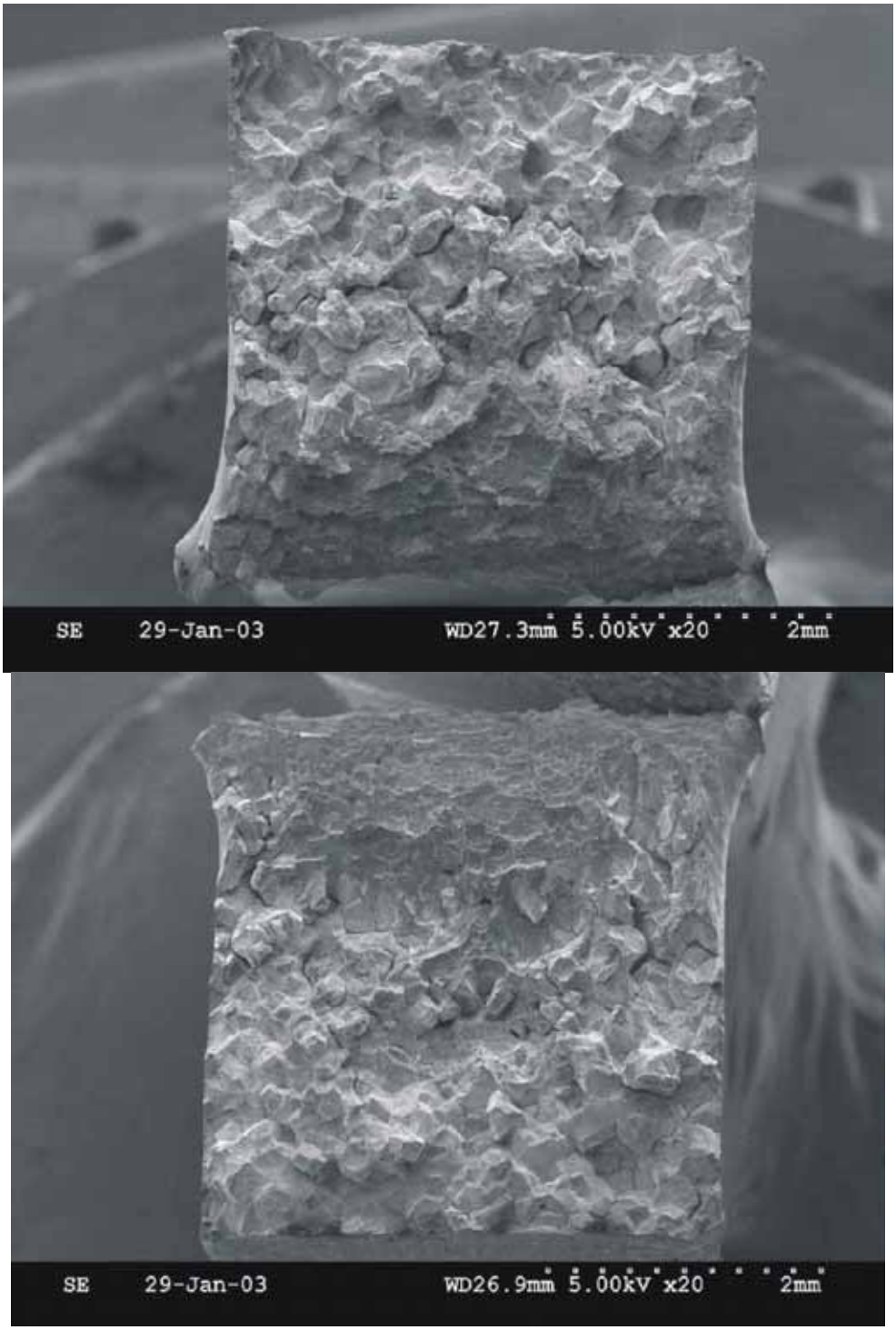

Figure 2.7.6: SE images of two halves of nozzle open crack sample. In-service cracking was intergranular in nature and extended a maximum ~0.12" deep. The laboratory fracture was ductile. 20X

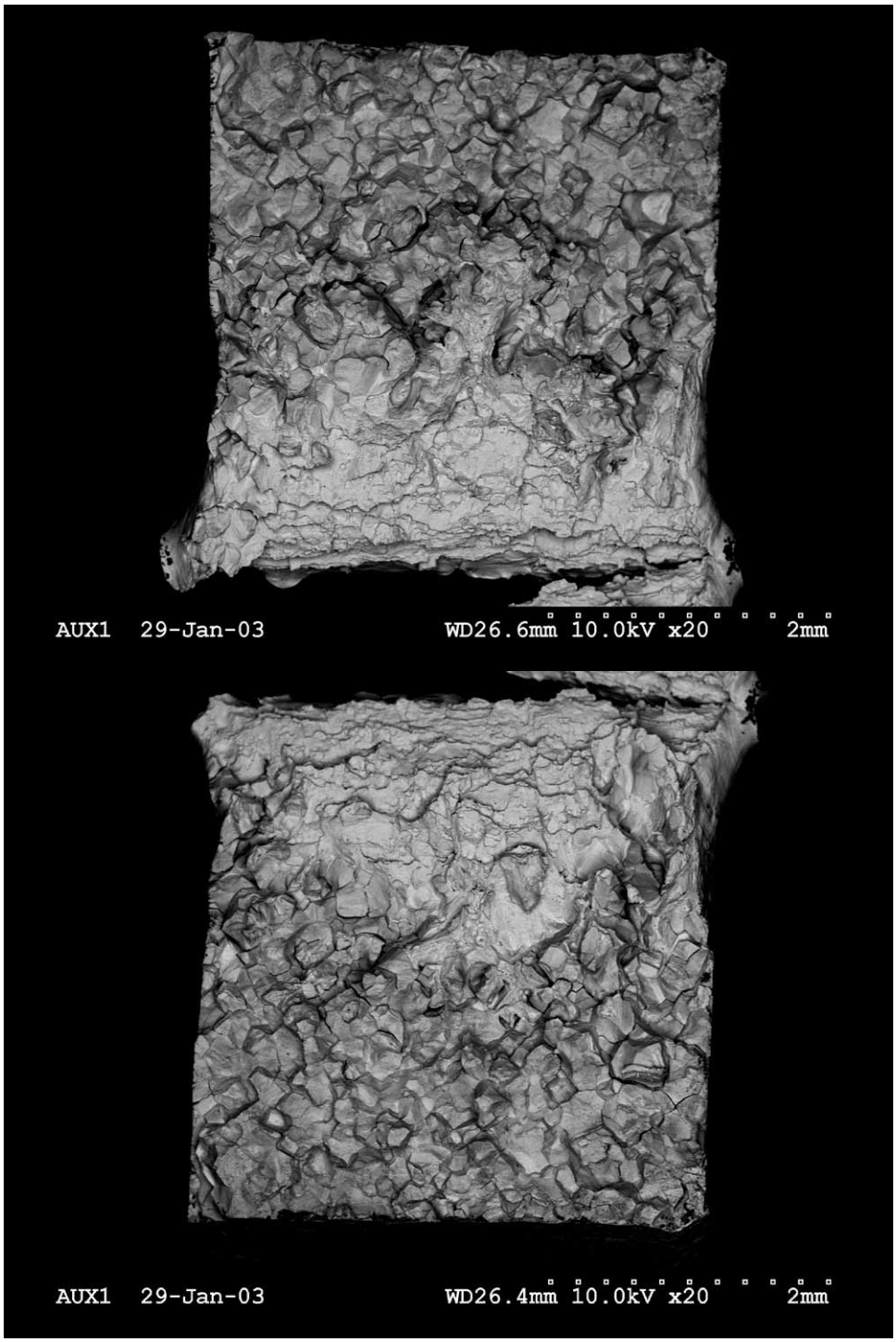

Figure 2.7.7: BSE images of two halves of nozzle open crack sample. The darker contrast of the in-service crack indicates the presence of an oxide layer (lab fracture is fresher) 20X

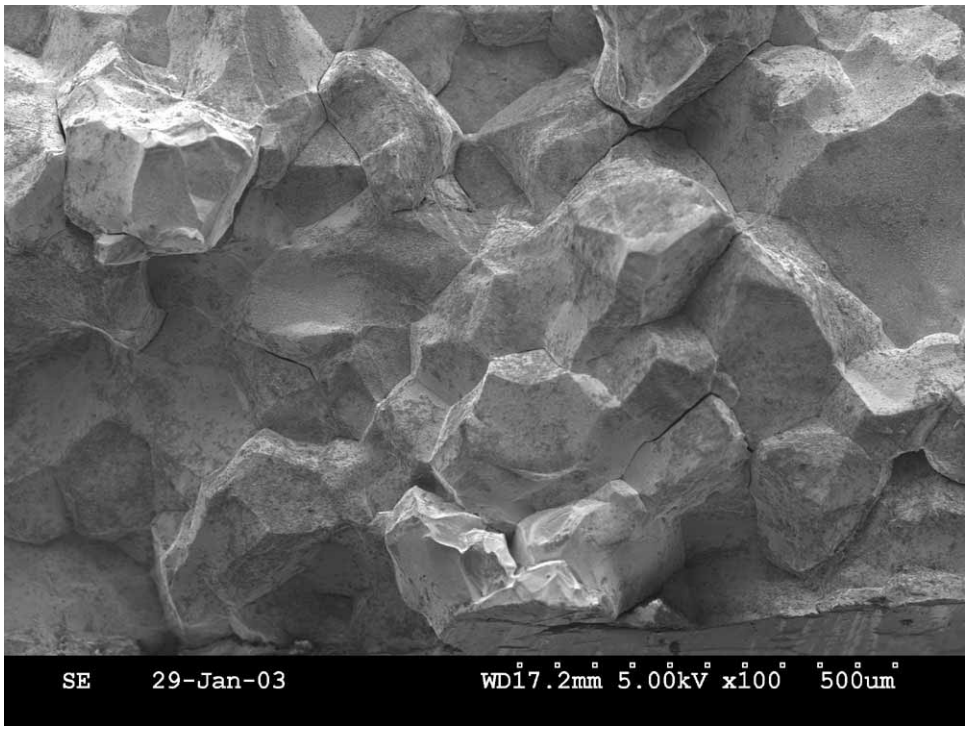

SE 100X

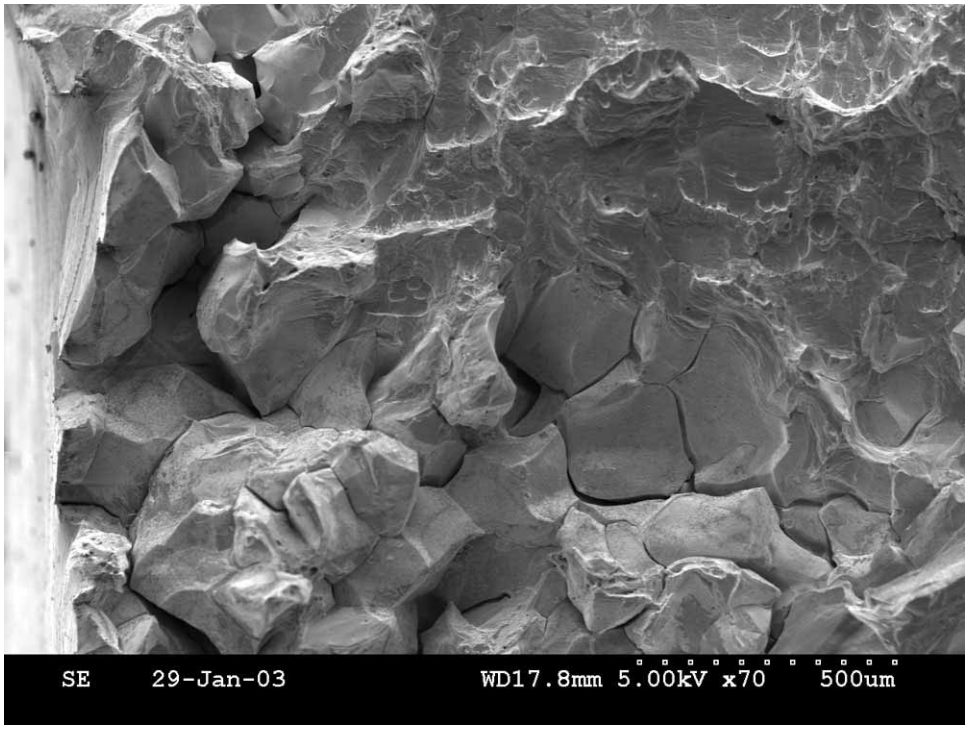

SE 70X

Figure 2.7.8: Micrographs showing typical intergranular appearance of in-service crack (top-near ID; bottom-at crack tip).

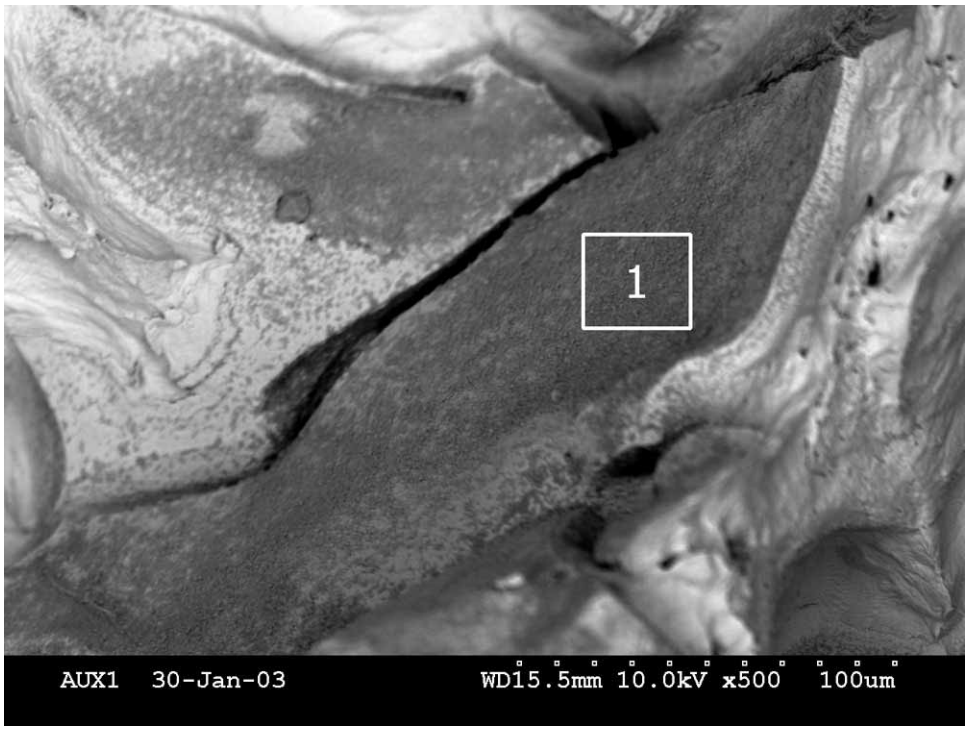

BSE image of intergranular facet showing area selected for EDS

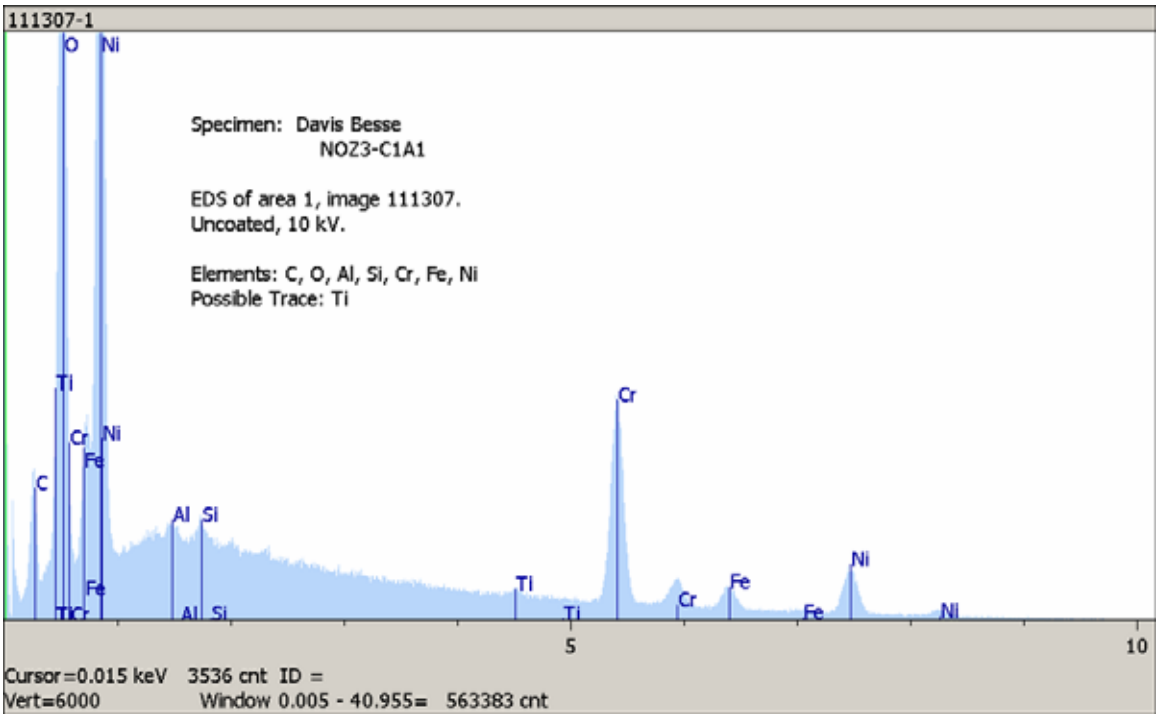

Figure 2.7.9: EDS spectrum collected from area 1 above. This area contained carbon, oxygen, aluminum, silicon, chromium, iron, and nickel, along with a trace amount of titanium.

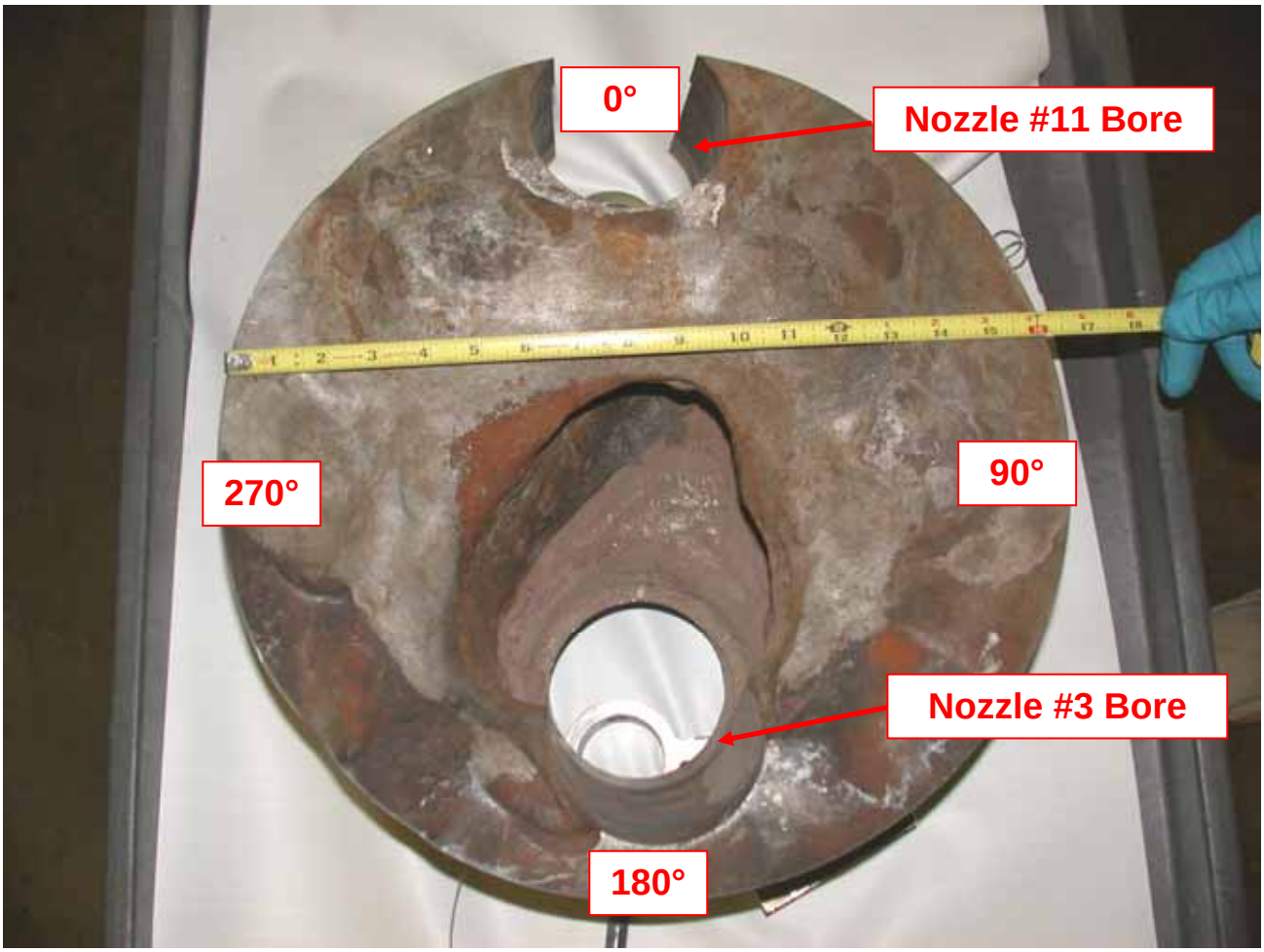

Figure 3.1.1: Top view of as-received cavity sample.

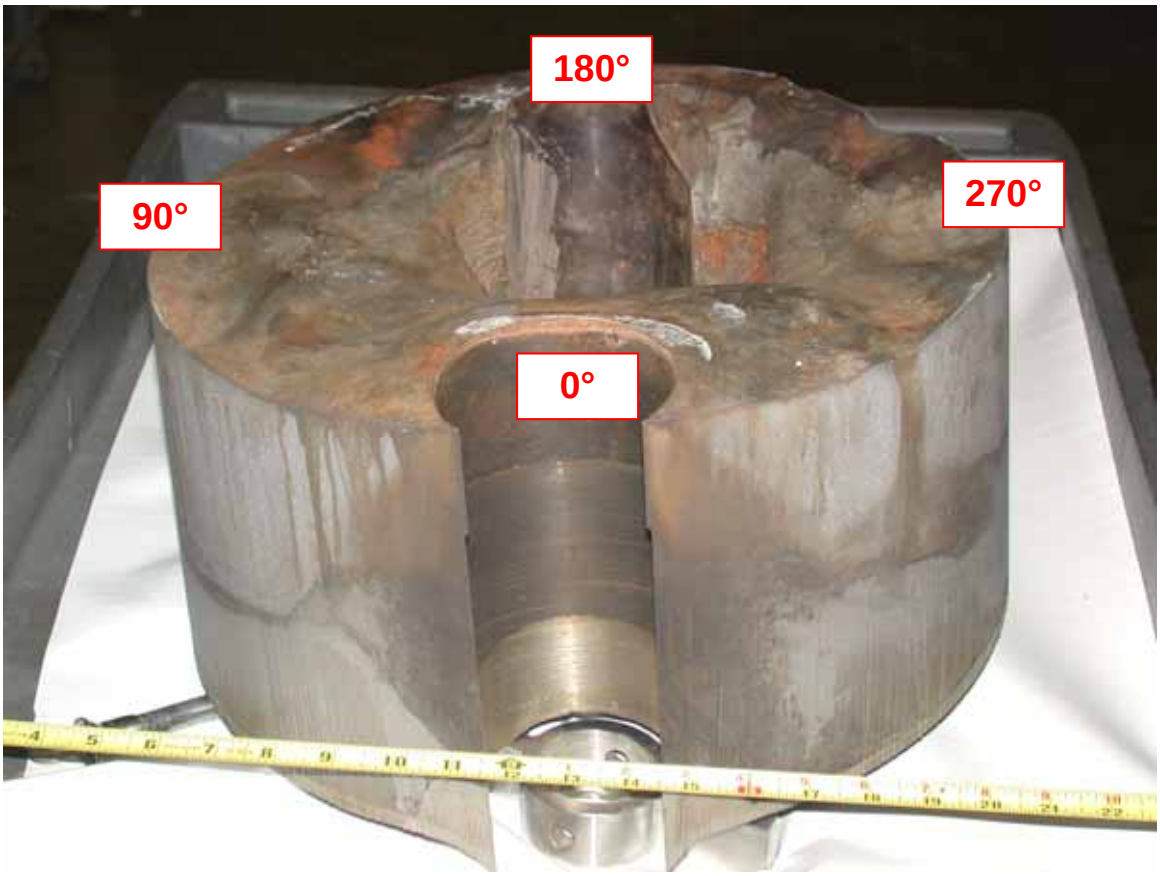

Figure 3.1.2: View of as-received cavity sample from nozzle #11 bore side.

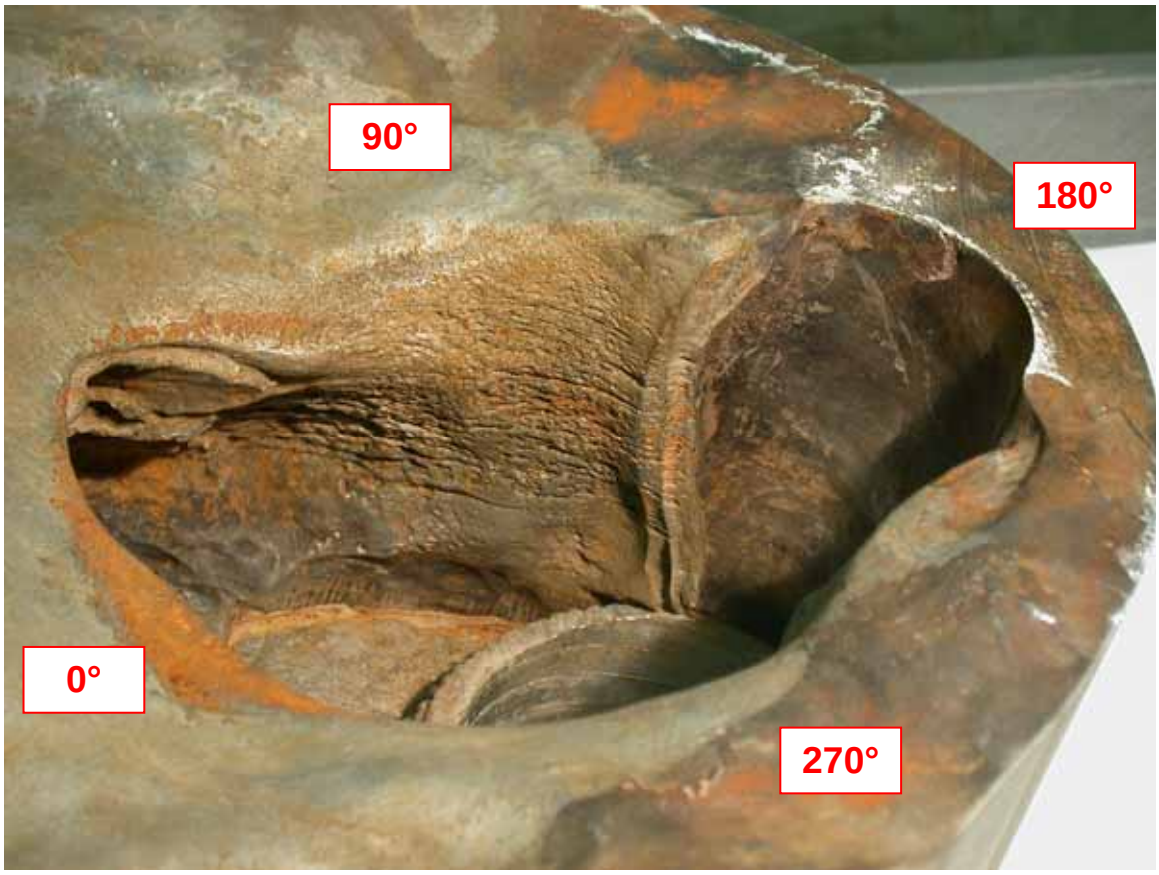

Figure 3.1.3: View of cavity looking toward 90°.

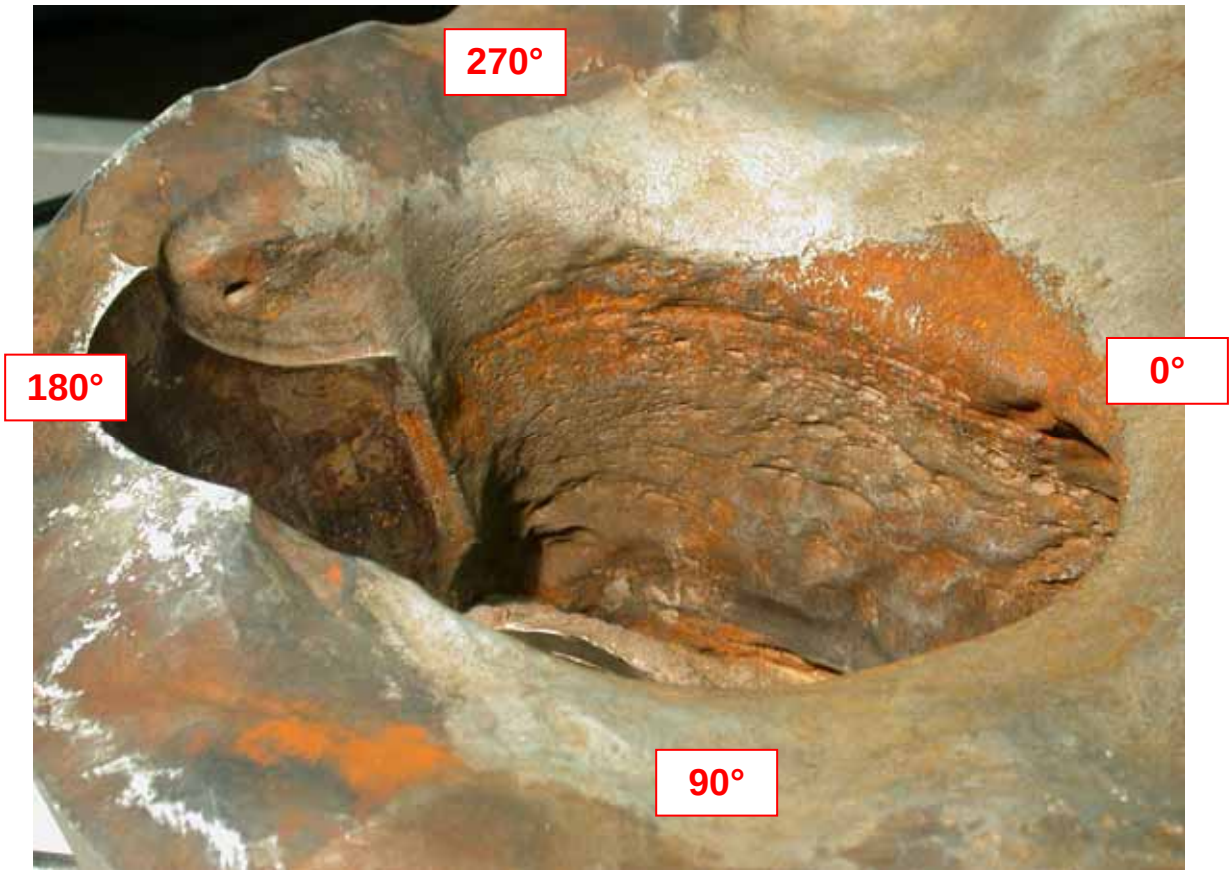

Figure 3.1.4: View of cavity looking toward 270°.

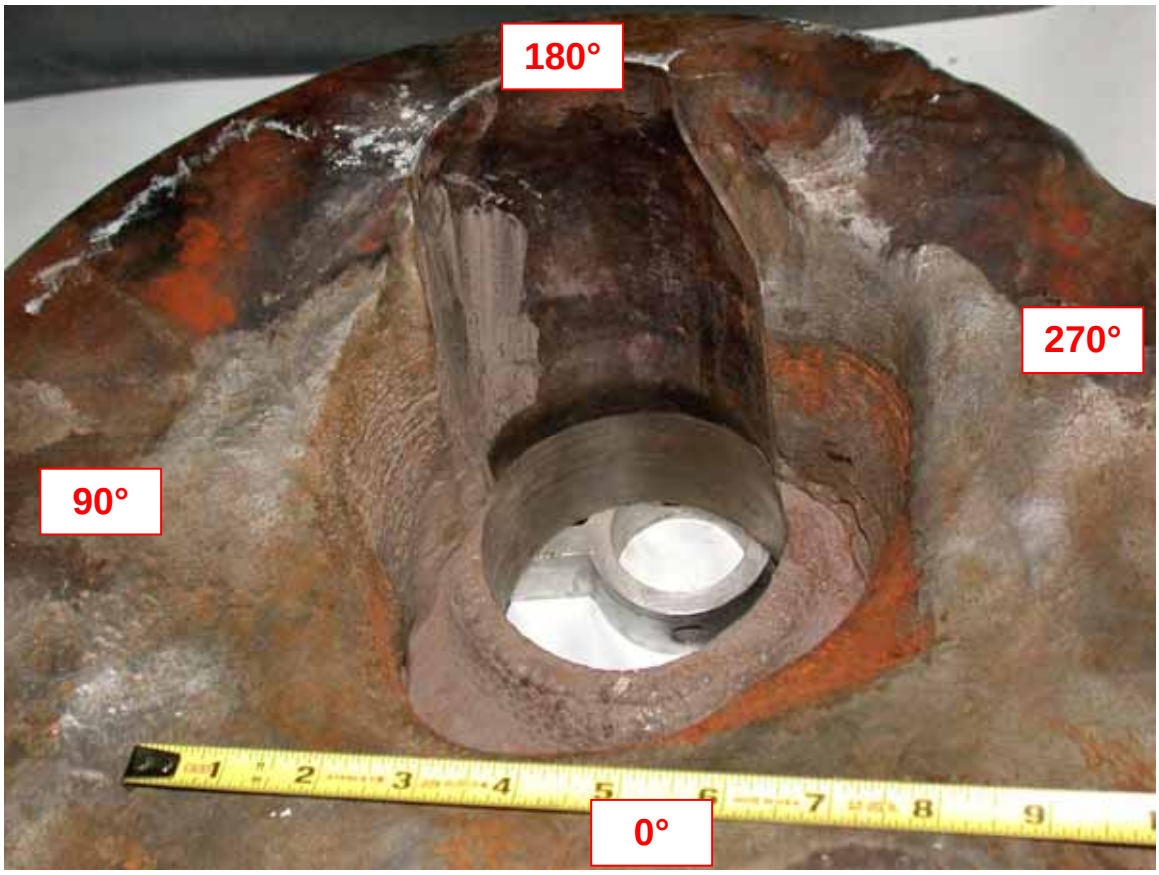

Figure 3.1.5: Looking toward 180°.

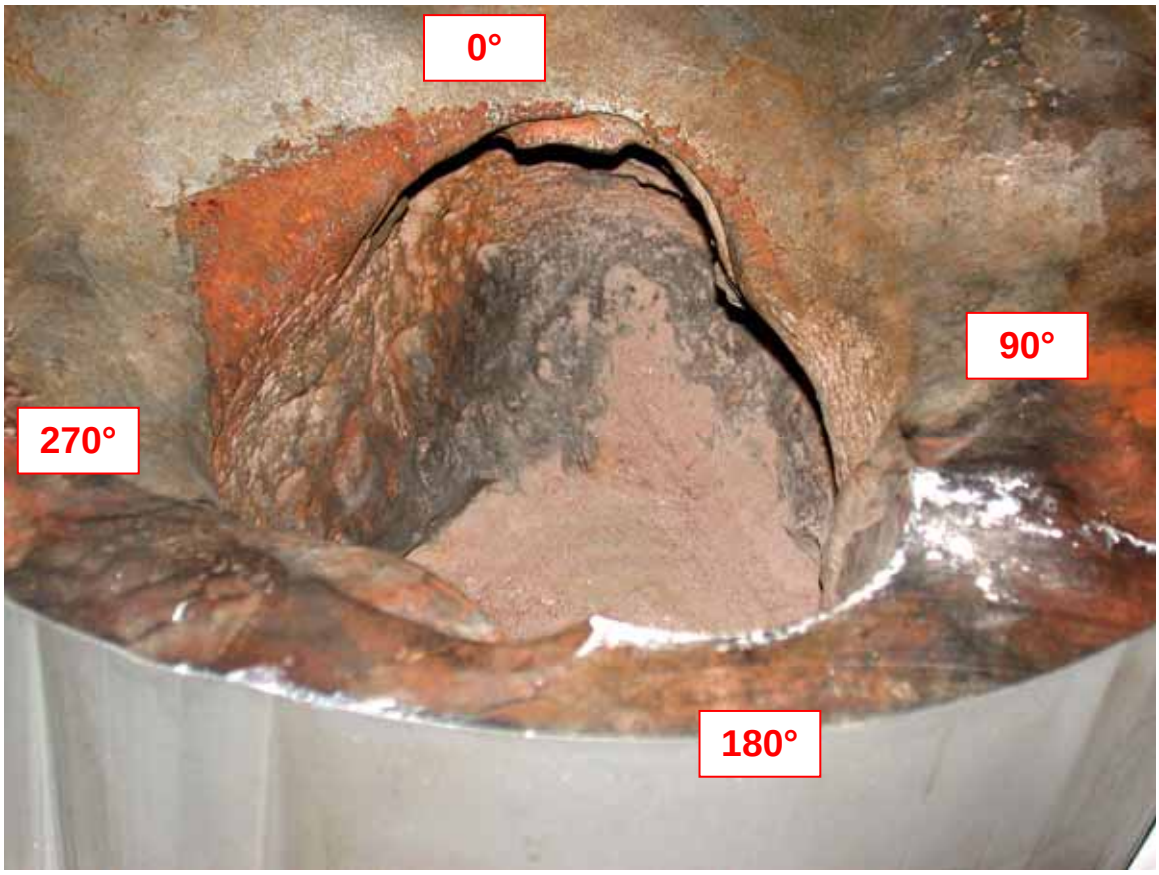

Figure 3.1.6: View of cavity looking toward nose (~10°).

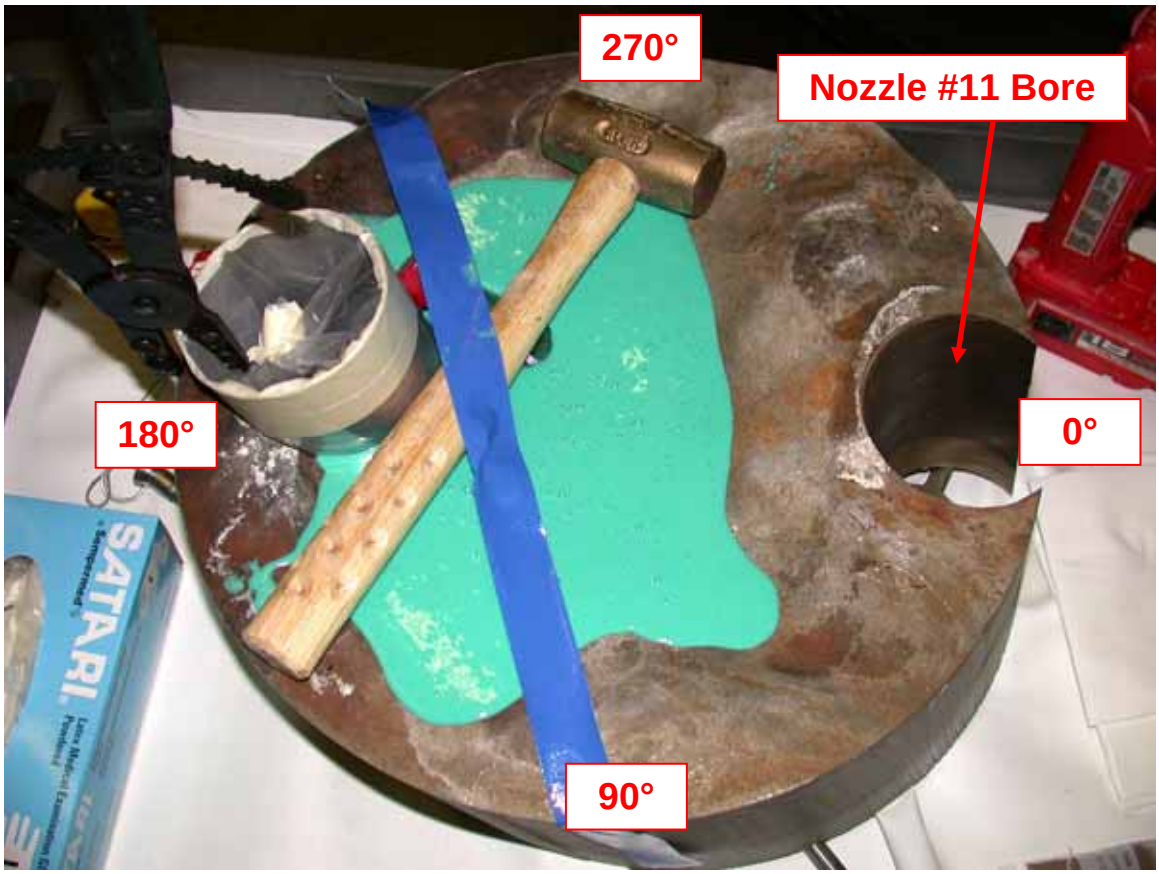

Figure 3.2.1: Photograph showing curing of cavity dental mold.

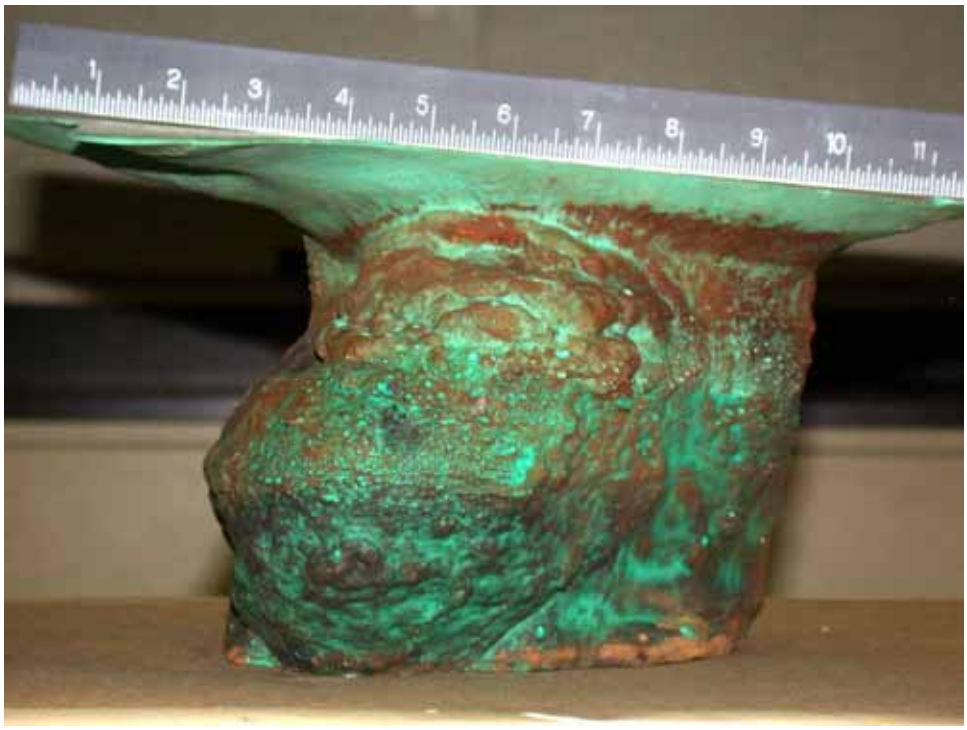

0°

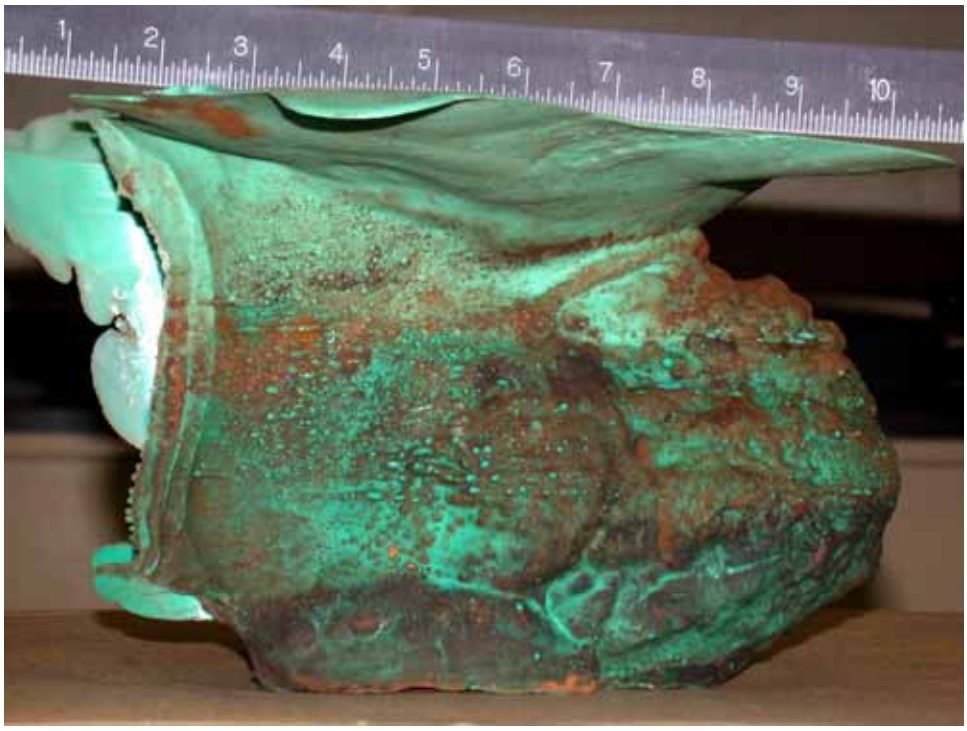

90°

Figure 3.2.2: Photographs of cavity dental mold.

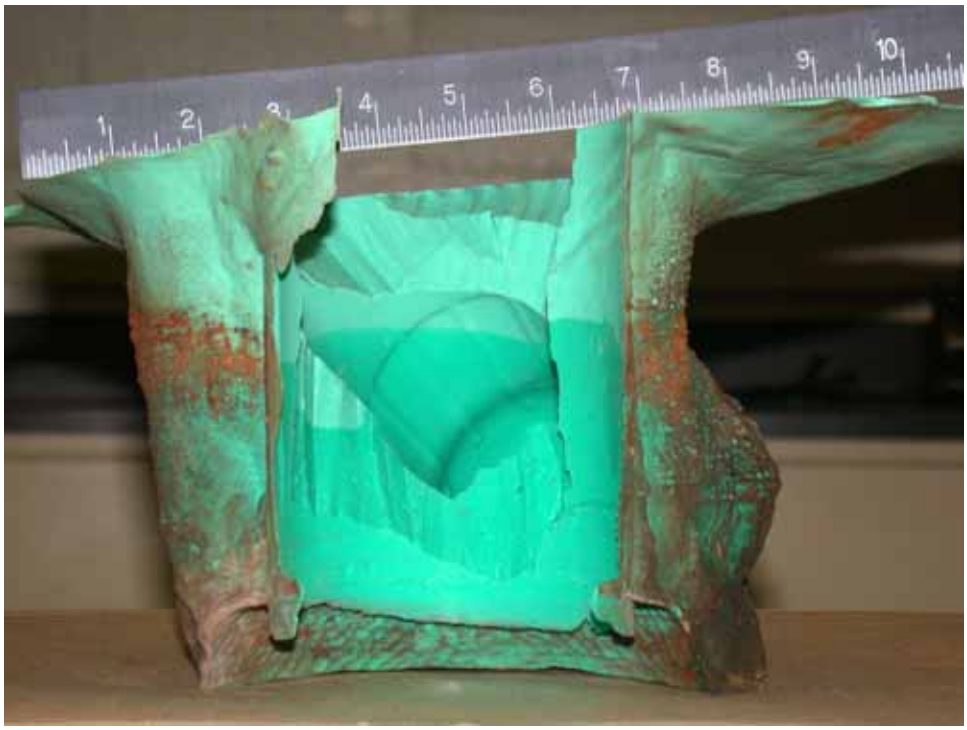

180°

270°

Figure 3.2.2 (cont.): Photographs of cavity dental mold.

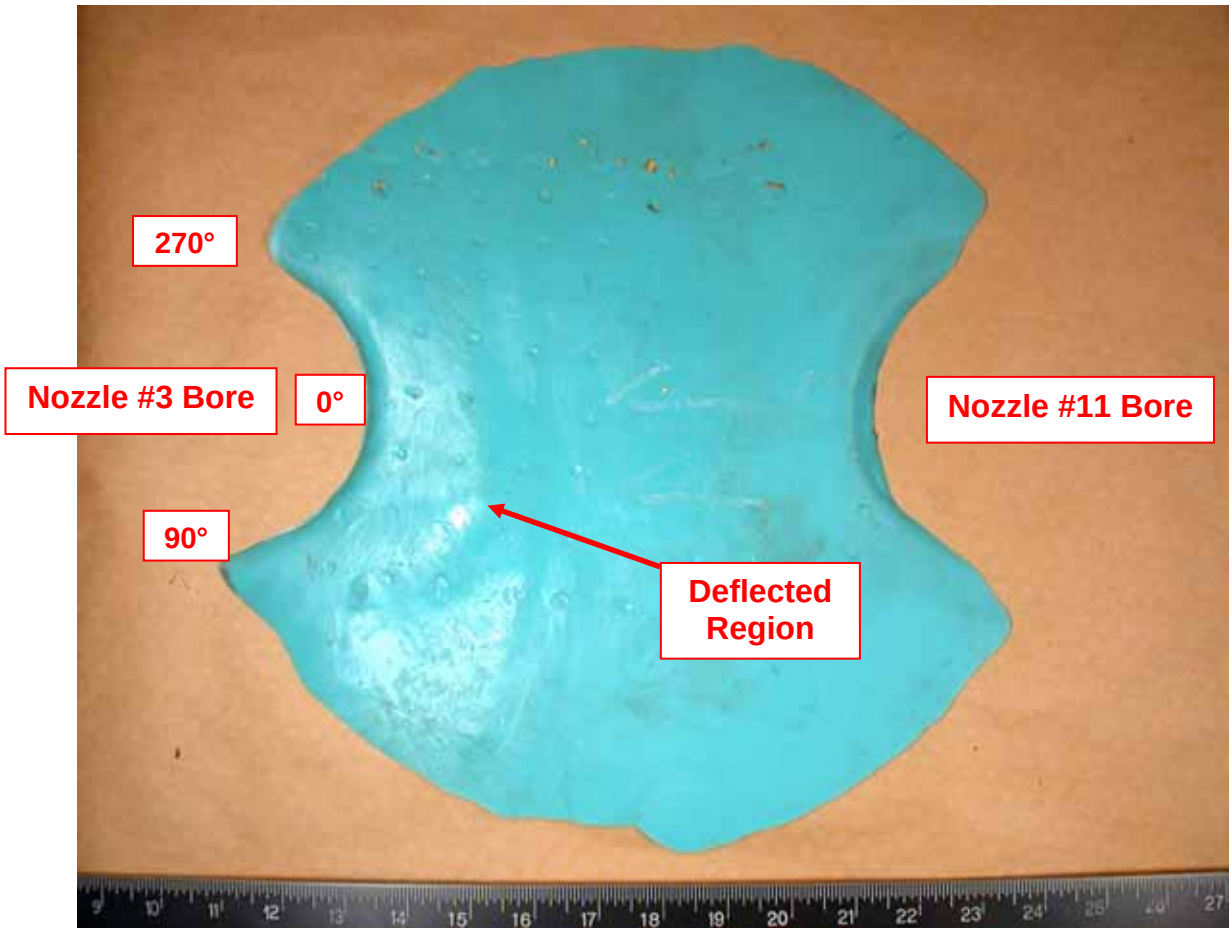

Figure 3.2.3: Photograph showing dental mold of RCS side of cladding.

Figure 3.3.1: Initial cavity sample section locations (cuts #1, #2, and #3).

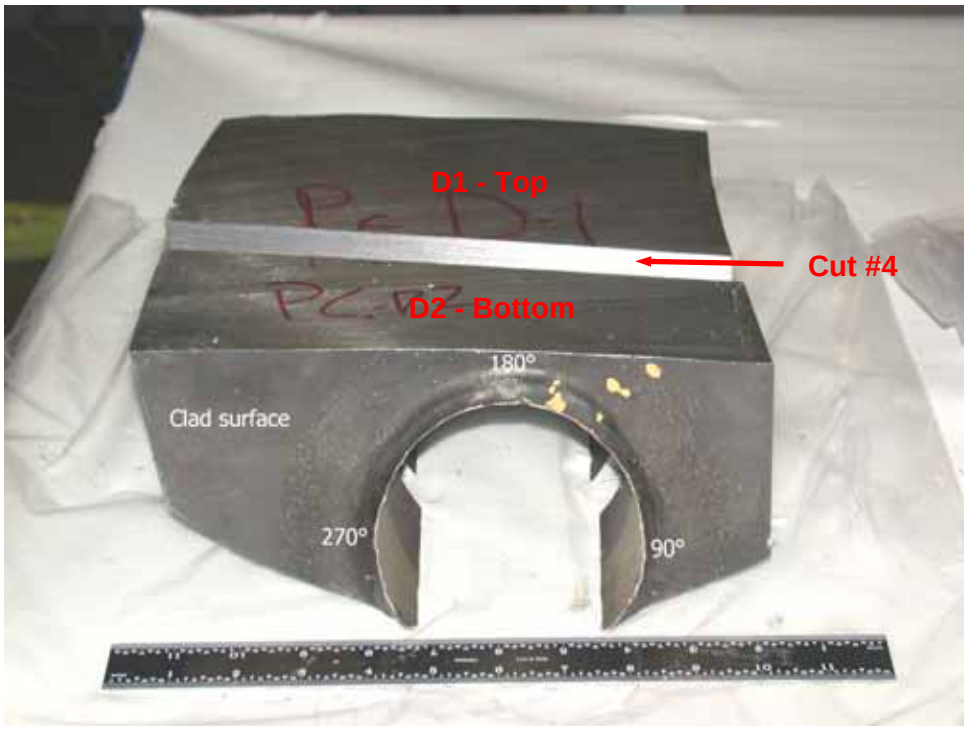

Cut #4 location

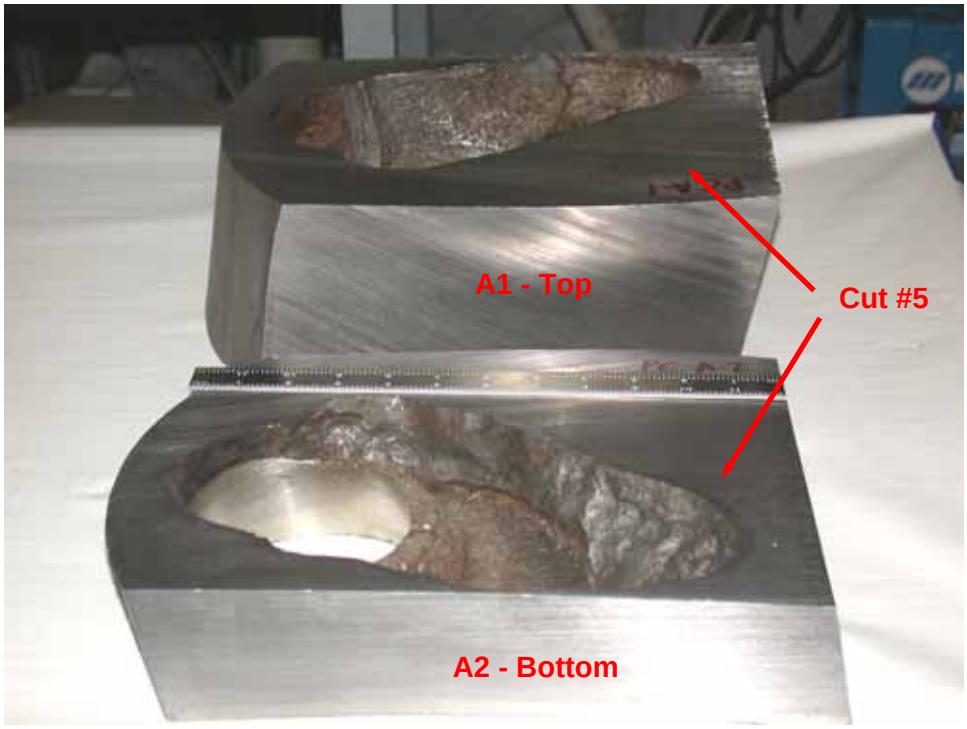

Cut #5 location

Figure 3.3.2: Photographs showing locations of cut #4 (top) and cut #5 (bottom). Piece A2 contained the exposed cladding.

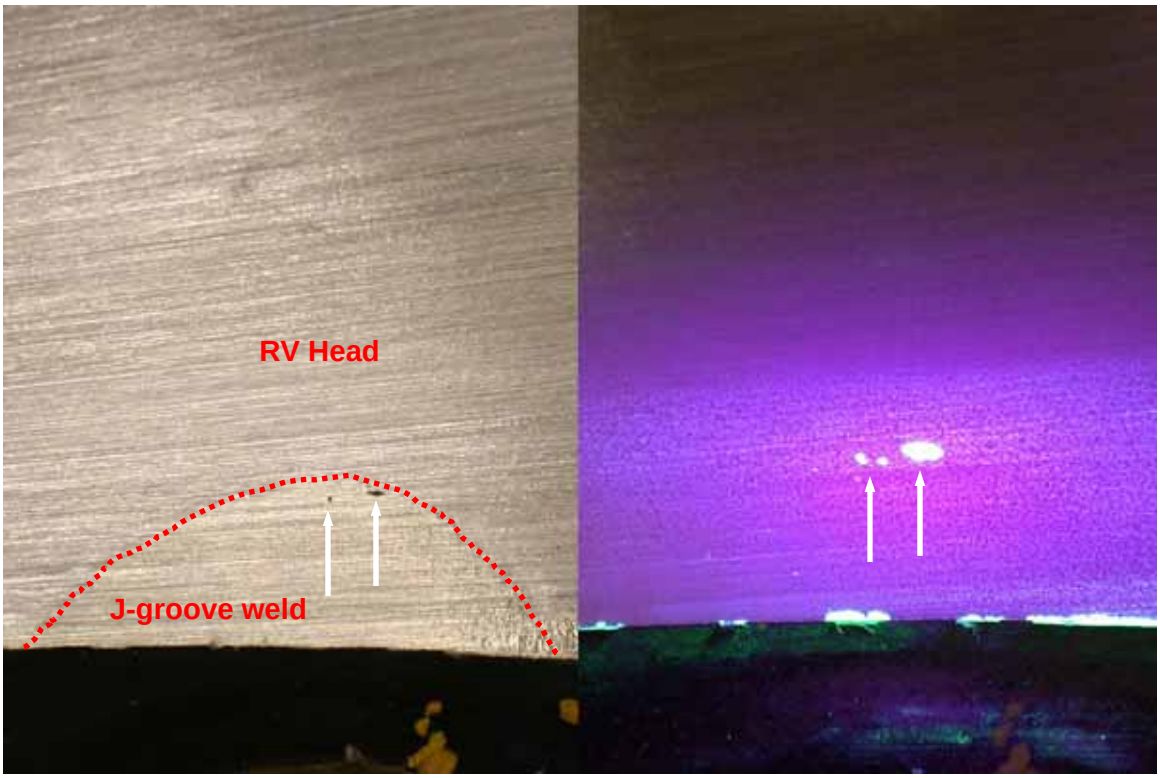

Figure 3.4.1: PT results for cut #3. A small weld void was present near the root of the nozzle #11 J-groove weld. Normal photo is on the left, black light photo on right. There was no evidence of cladding disbond noted on any of the cut faces examined. ~1X

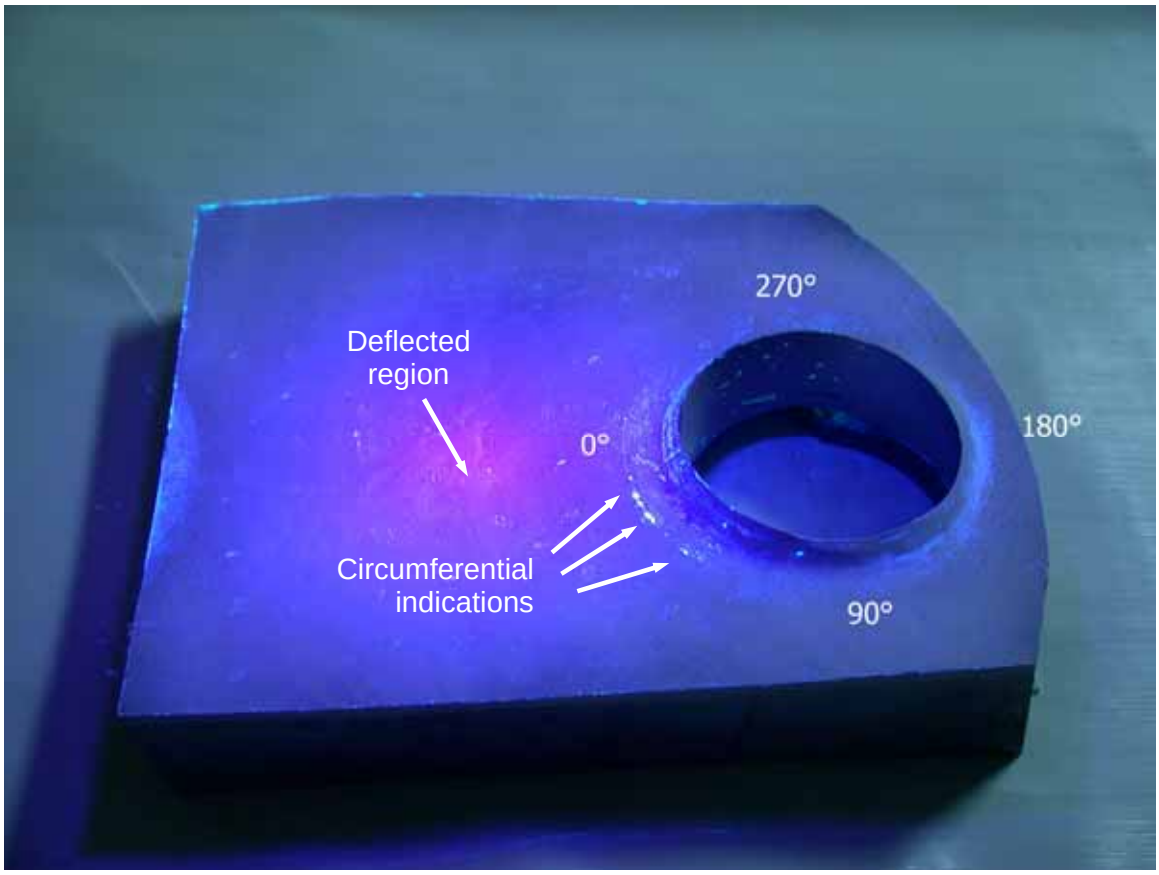

Figure 3.4.2: Circumferential indications on RCS side of cladding from ~0° to 45°. No indications were present in the upward-deflected region of the cladding.

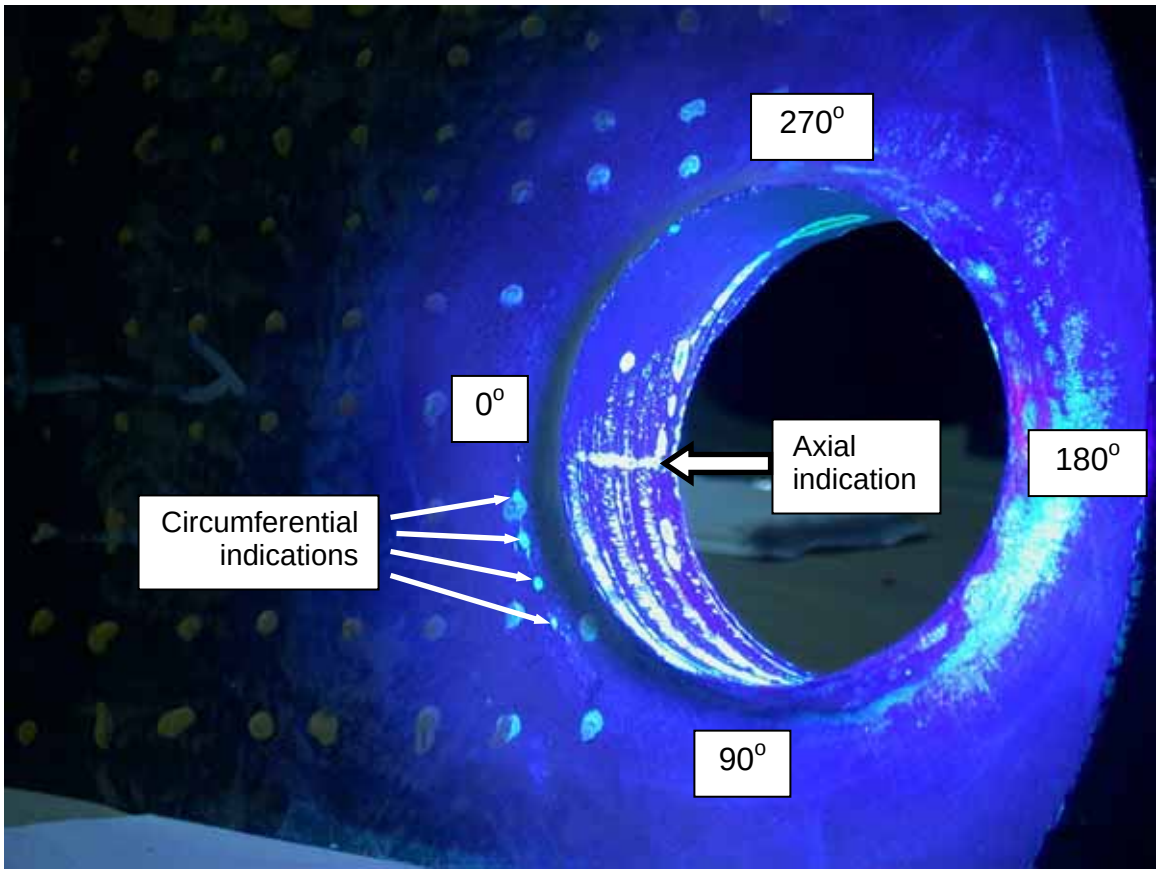

Figure 3.4.3: PT results for nozzle #3 J-groove weld bore and cladding underside. The J-groove weld contained an axial indication near 10° on the bore ID and circumferential indications on the RCS side from ~20° to ~45°.

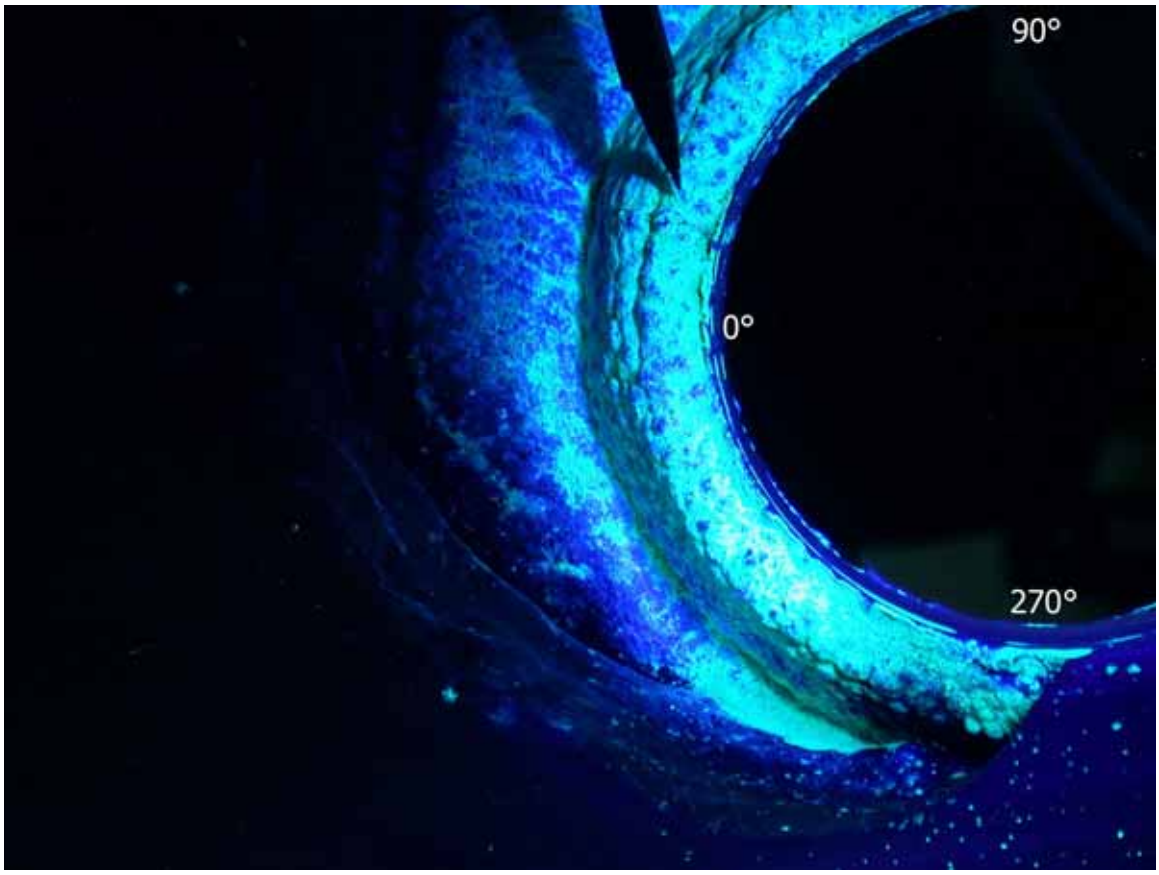

Figure 3.4.4: PT results for upper surface of exposed J-groove weld. The axial crack is visible near 10° (rough weld texture produced high PT background).

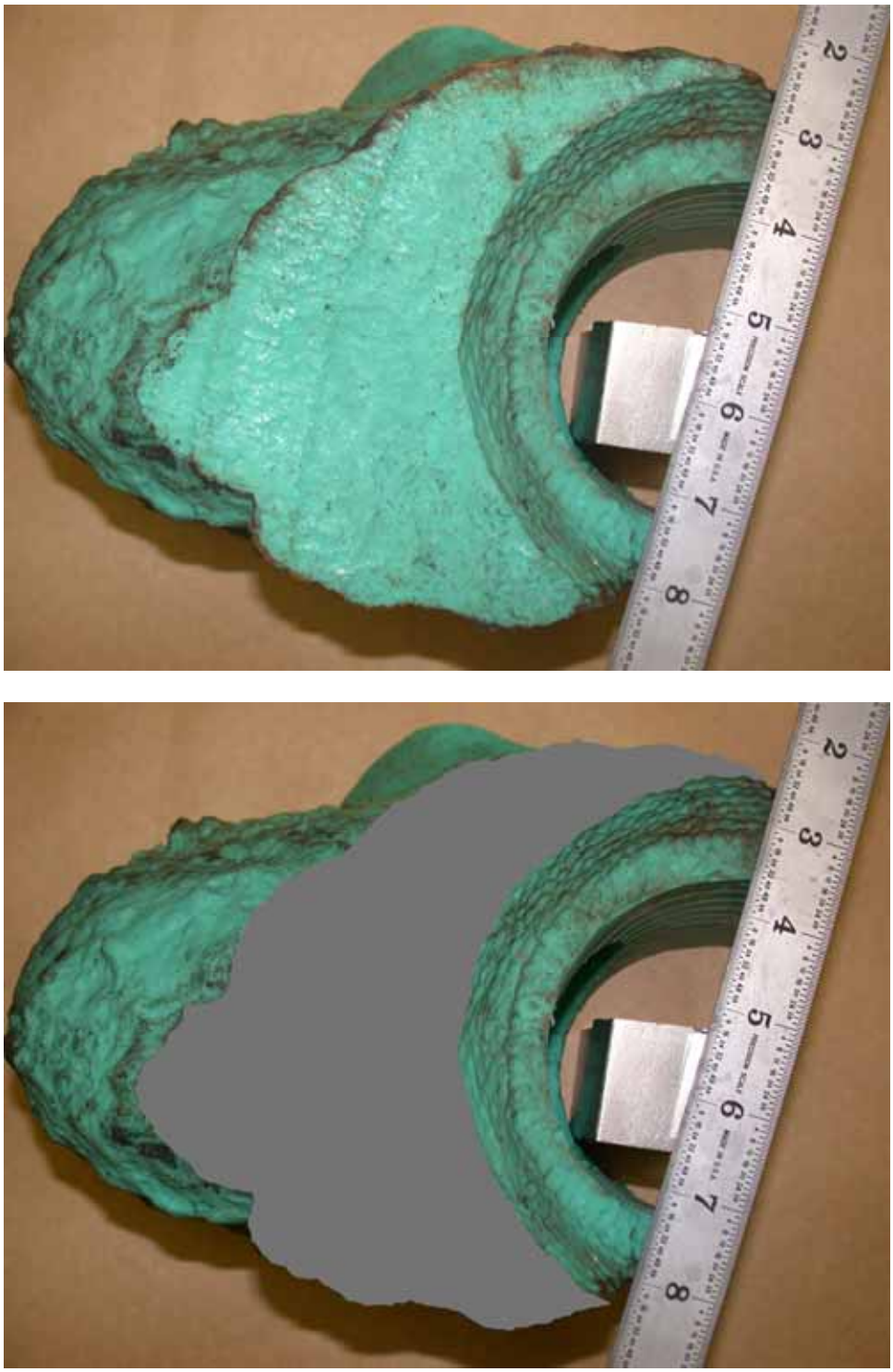

Figure 3.5.1: Photographs showing exposed cladding surface. The gray mask in the lower photograph was used to calculate the exposed cladding surface area.

Figure 3.5.2: Photographs showing clad thickness setup (top) and coordinate system (bottom).

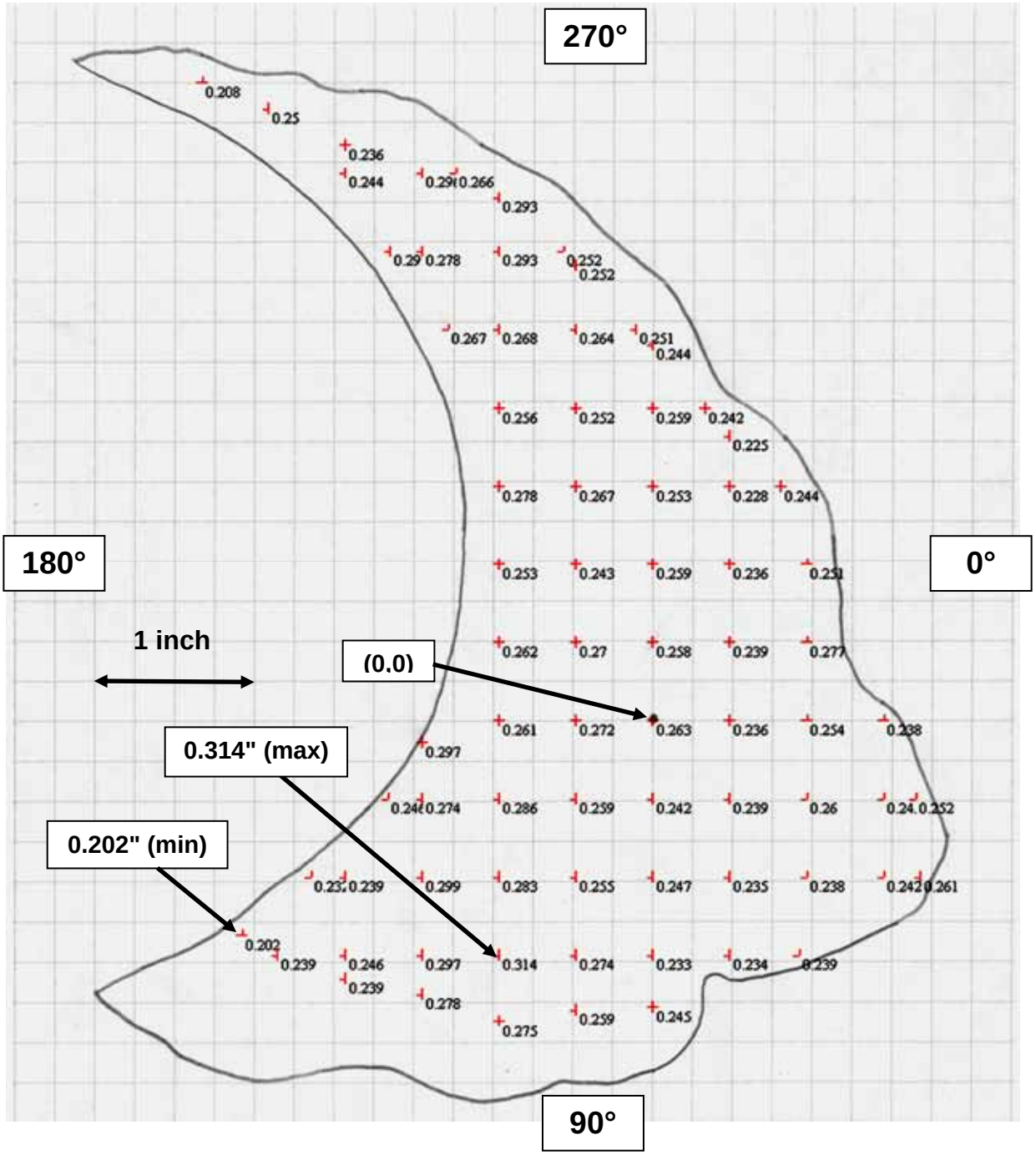

Figure 3.5.3: Cladding thickness measurements.

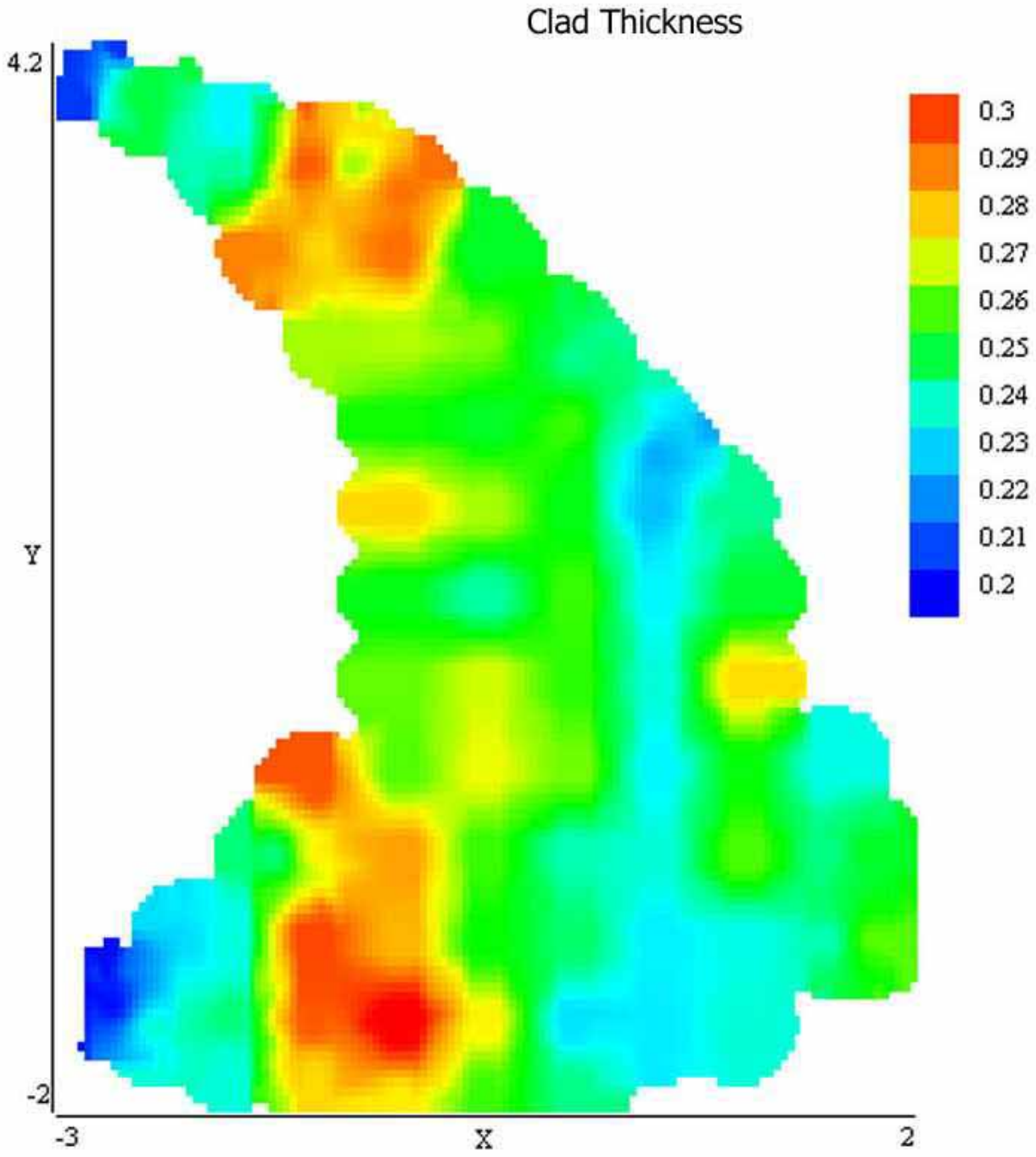

Figure 3.5.4: Colorized representation of clad thickness measurements.

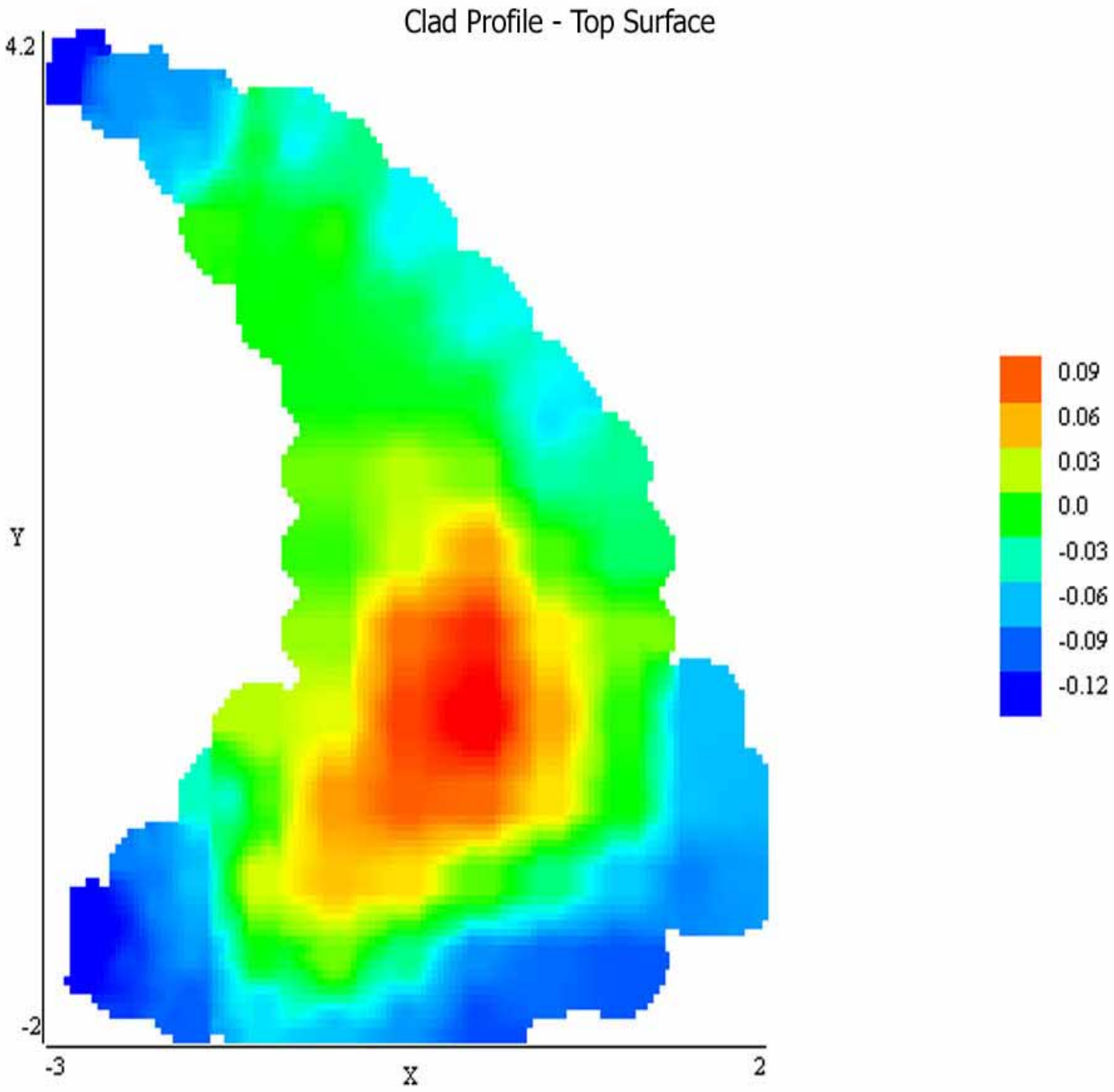

Figure 3.5.5: Colorized representation of exposed cladding profile. Red area denotes area of maximum deflection.

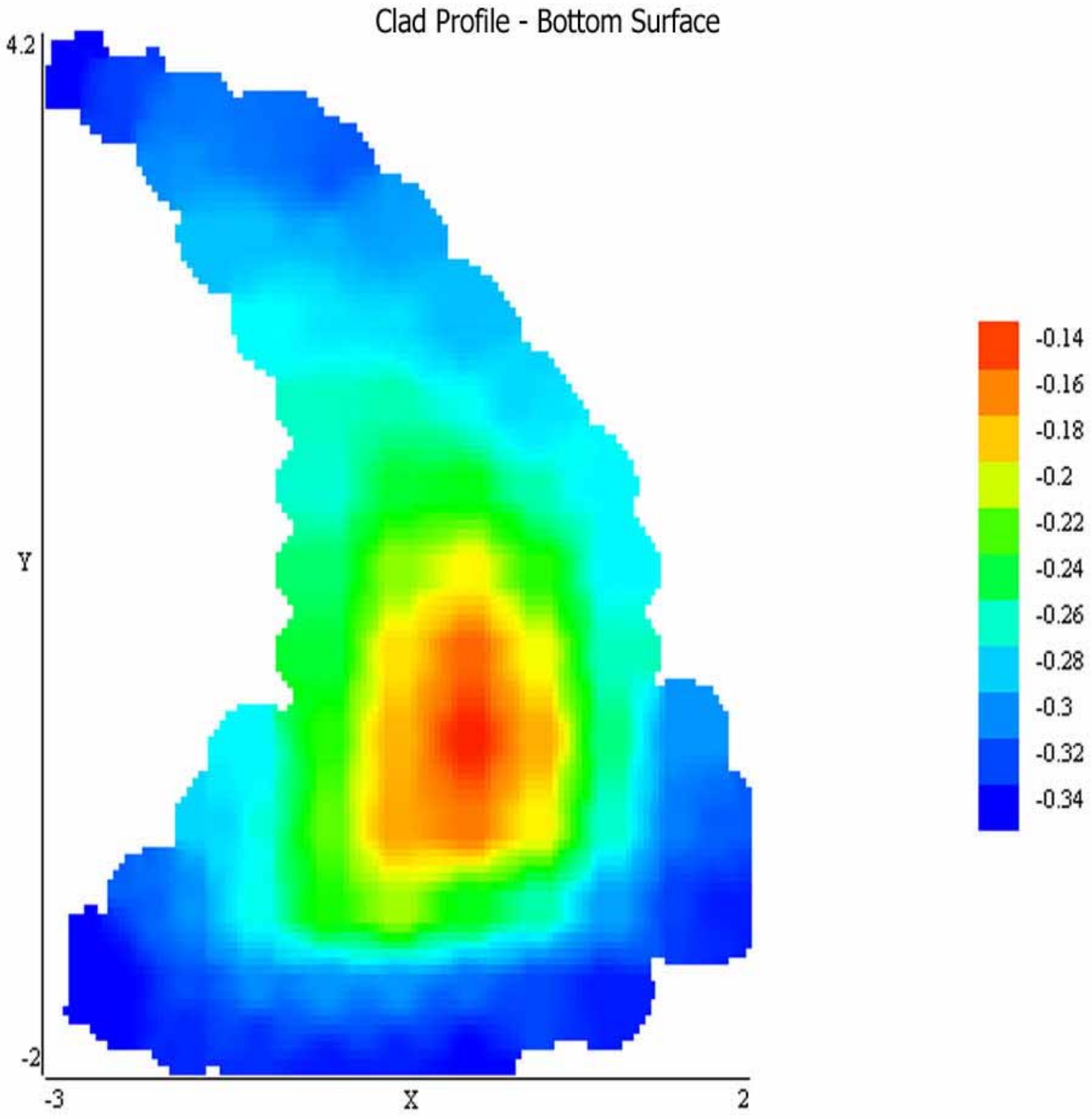

Figure 3.5.6: Colorized representation of bottom surface of cladding (RCS side). Red area denotes area of maximum deflection.

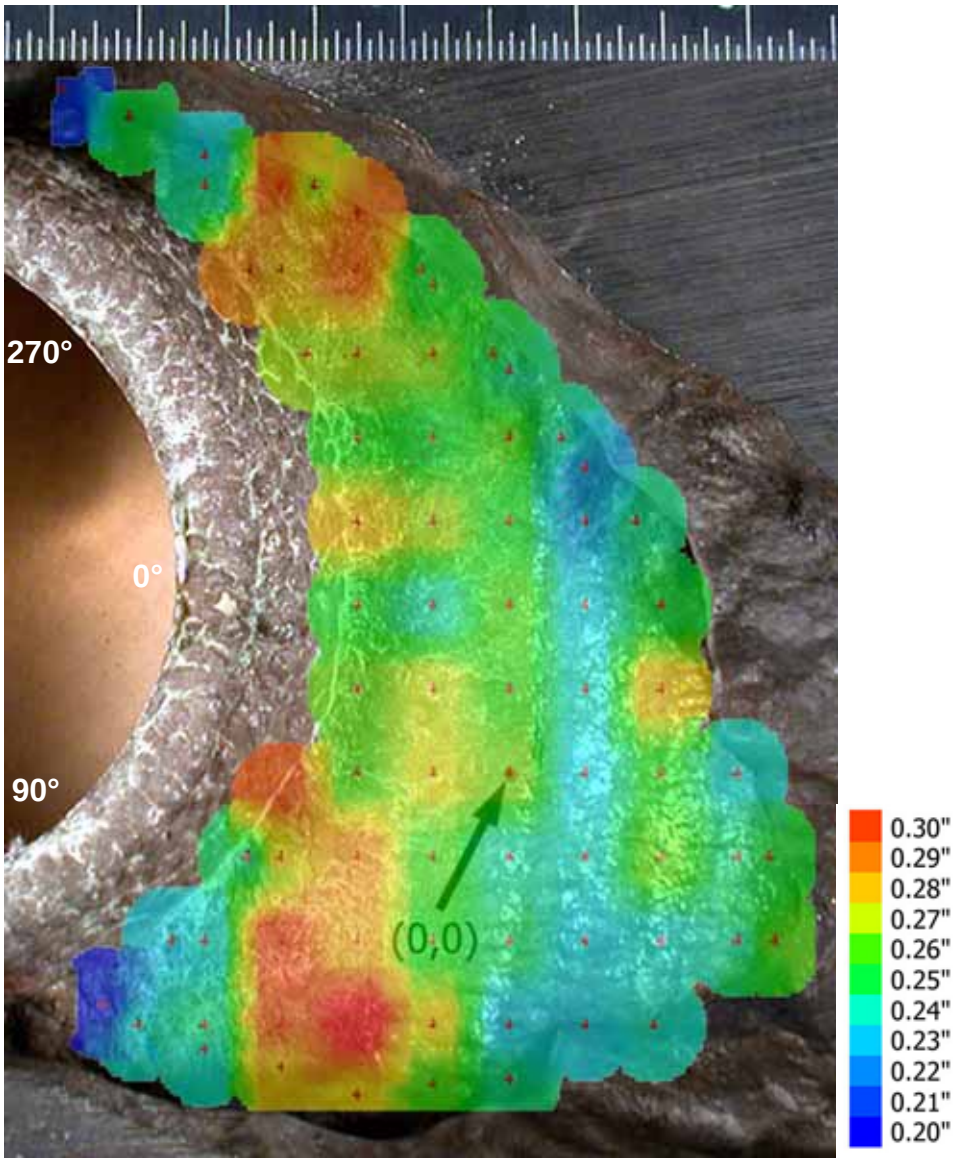

Figure 3.5.7: Exposed cladding surface with superimposed colorized thickness data. The thinnest areas of cladding occurred adjacent to the J-groove weld toward the 90° (0.202") and 270° (0.208") locations.

Figure 3.6.1: Photograph showing crack in exposed cladding in deflected region. Red dot indicates (0, 0) coordinates for thickness measurements.

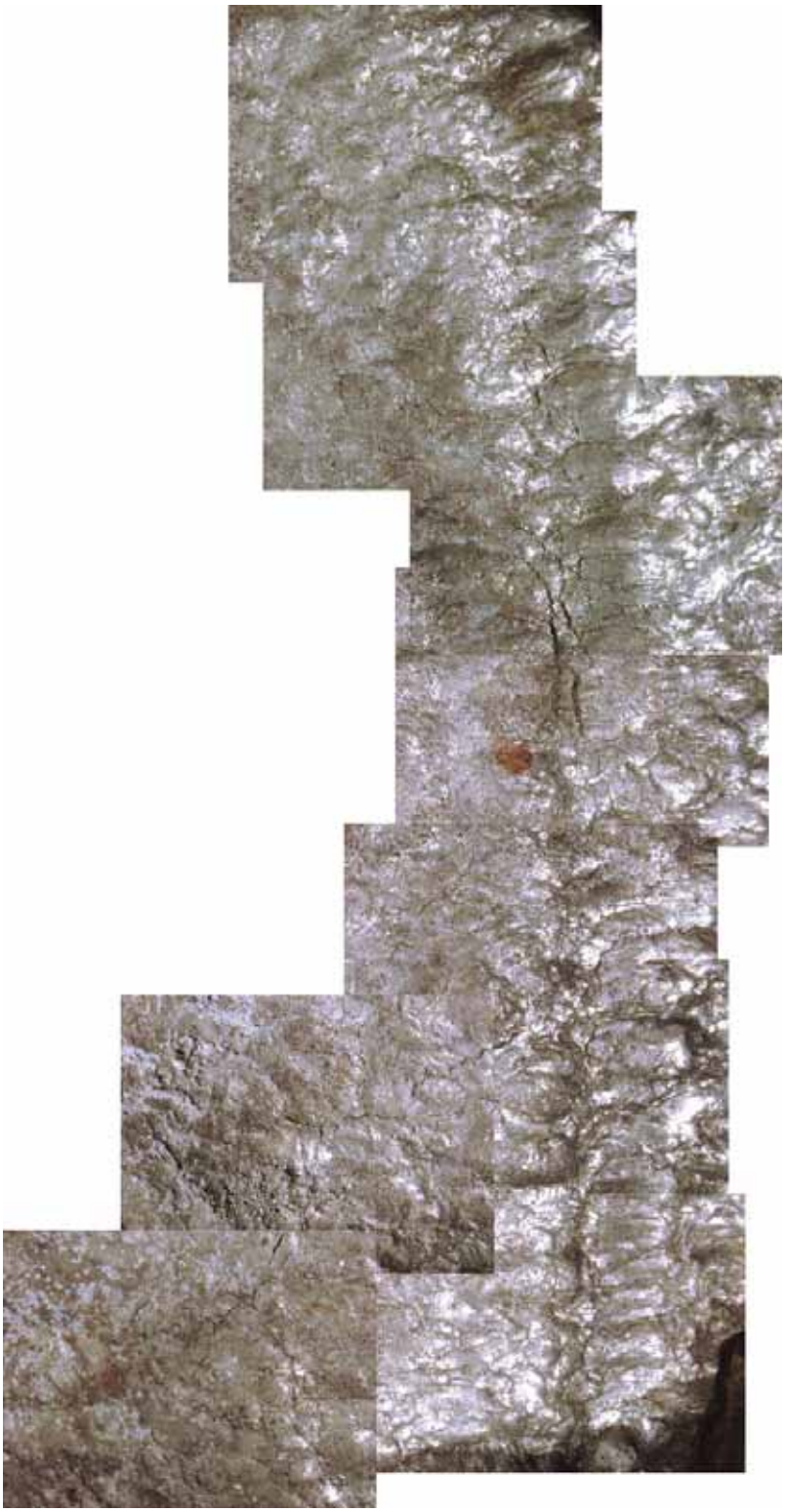

Figure 3.6.2: Mosaic showing cracking in exposed cladding. 2X

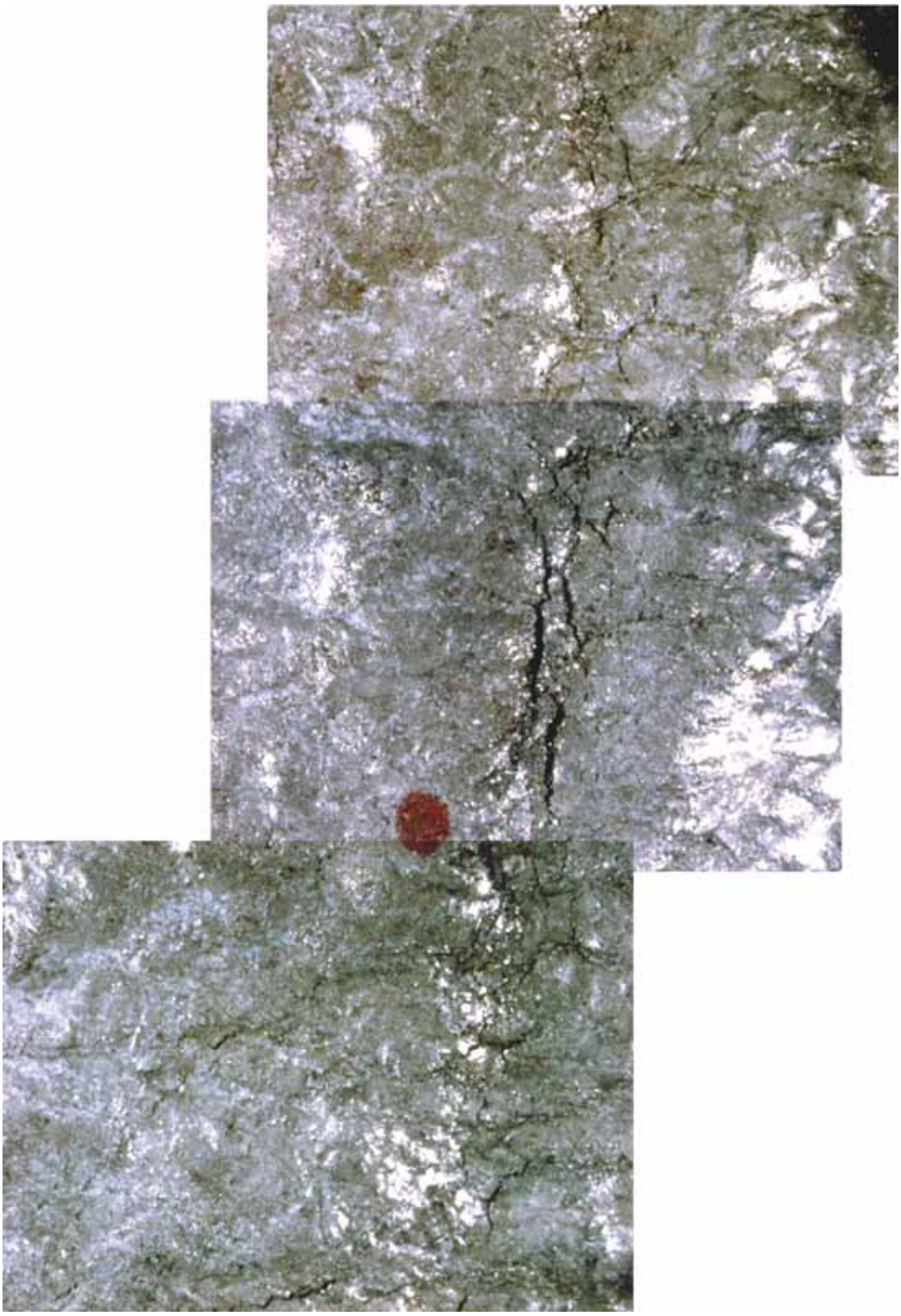

Figure 3.6.3: Higher magnification view of cladding crack in bulged region. ~4X

Figure 3.6.4: Higher magnification photograph of crack near center bulge. 25X

Figure 3.6.5: Low magnification photograph of the cavity underside. The red circle shows the area of maximum deflection. The white dots were applied at Davis-Besse for the UT thickness measurements. The two parallel lines toward the left indicate the Nozzle 11 position, which is outside the photo on the left. This maximum bulging area is shown at higher magnification in the next figure.

~0.9X

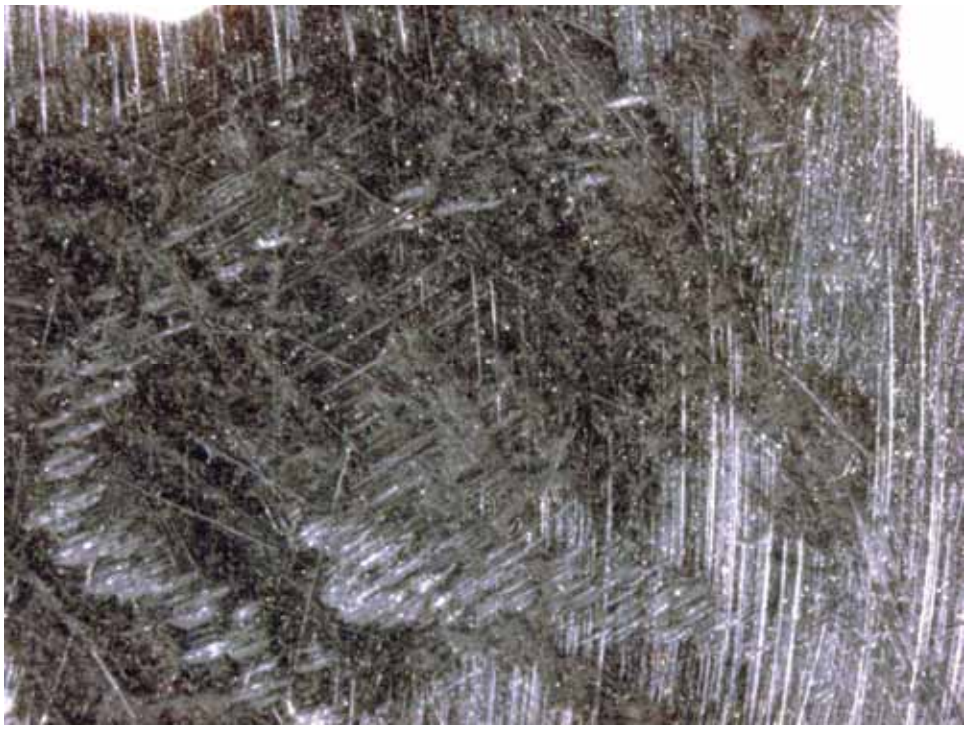

5X

Figure 3.6.6: Higher magnification photographs of cavity underside in area of maximum deflection. No cracks were observed in this area.

Looking at J-groove weld bore near 10°. ~1.2X

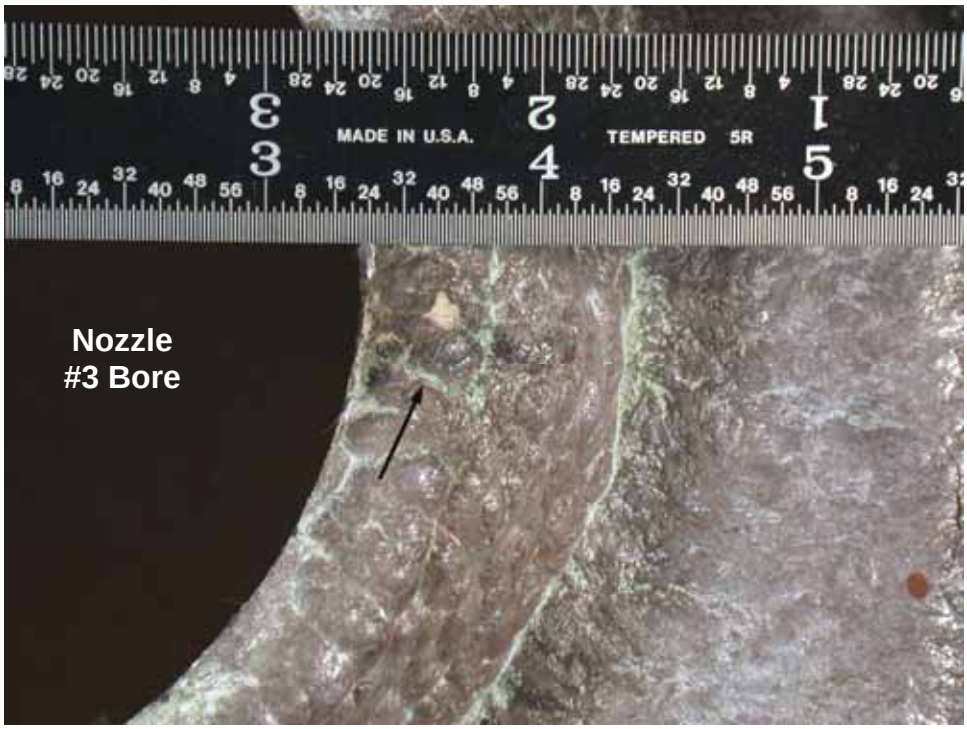

Top view of J-groove weld crack near 10°. ~1.4X

Figure 3.6.7: Photographs showing axial crack in nozzle #3 J-groove weld near 10°.

Figure 3.6.8: Axial cracks located on J-groove weld bore near 180°. ~0.75X

Looking toward 90° ~0.7X

Looking toward 270° ~0.5X

Figure 3.6.9: Low magnification photographs of cavity sidewall.

Sidewall detail near 90° (nozzle #3 bore to right). ~1X

Sidewall detail near 270° (nozzle #3 bore to lower left). ~1.2X

Figure 3.6.10: Higher magnification photographs taken near the nozzle #3 bore.

Detail of side wall near 270°. ~1.7X

Looking up at cavity nose. ~0.7X

Figure 3.6.11: Photographs showing the cavity sidewall near 270° (top) and looking up at the cavity nose (bottom).

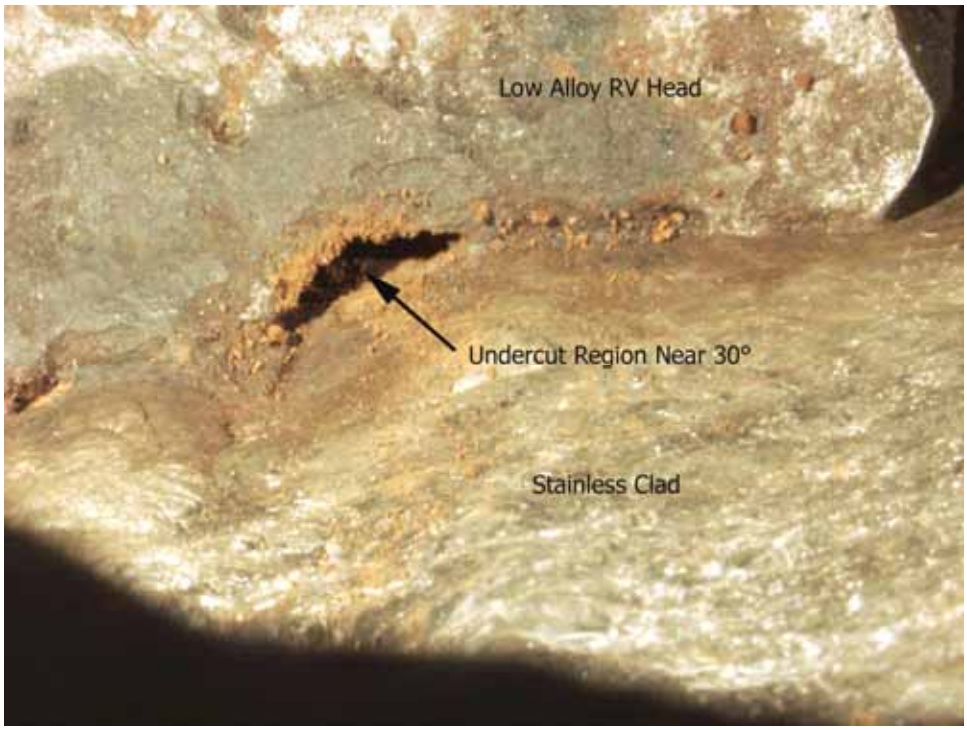

Near 30° 5X

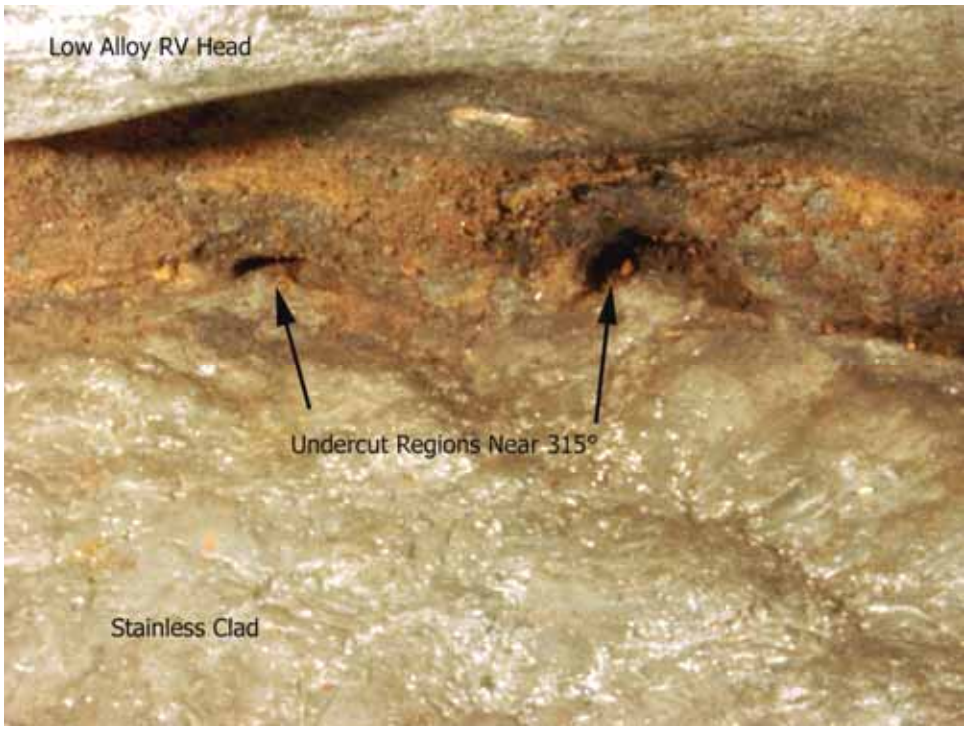

Near 315° 5X

Figure 3.6.12: Photographs showing undercut regions of cavity near 30° (top) and 315° (bottom).

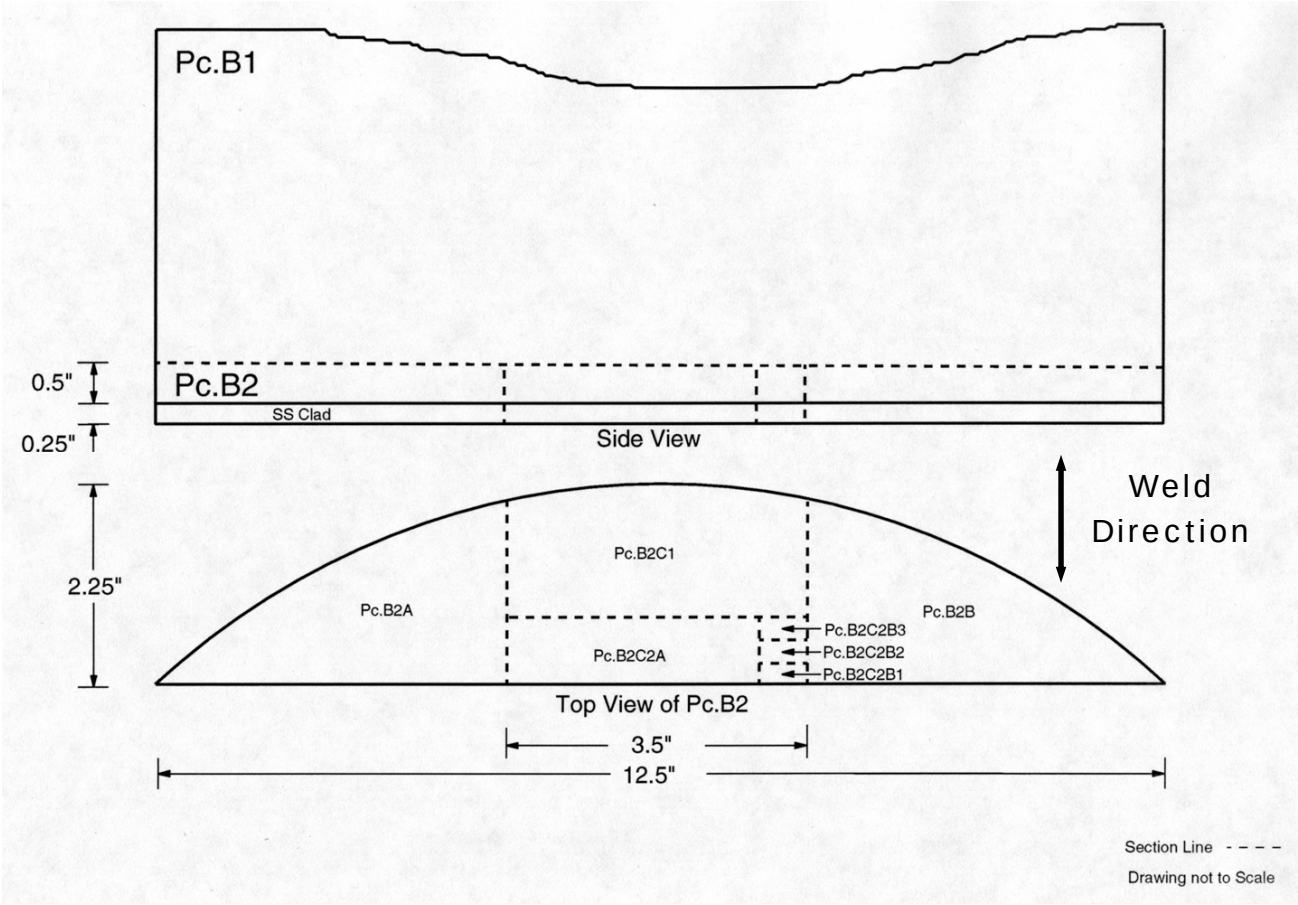

Figure 4.1.1: Schematic showing section locations and sample identifications for Block "B".

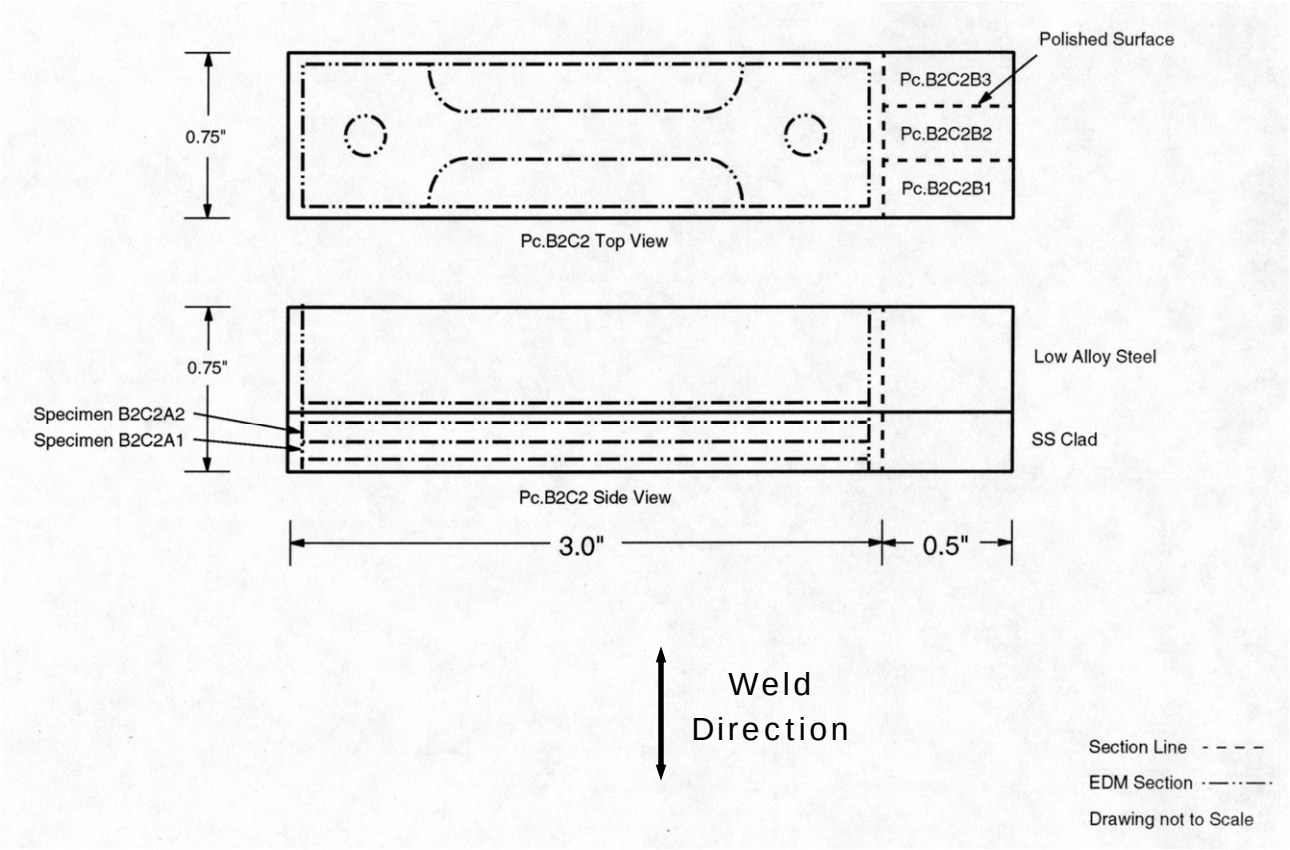

Figure 4.1.2: Schematic showing tensile specimen locations. The polished surface of piece B2C2B3 (met sample) is also indicated.

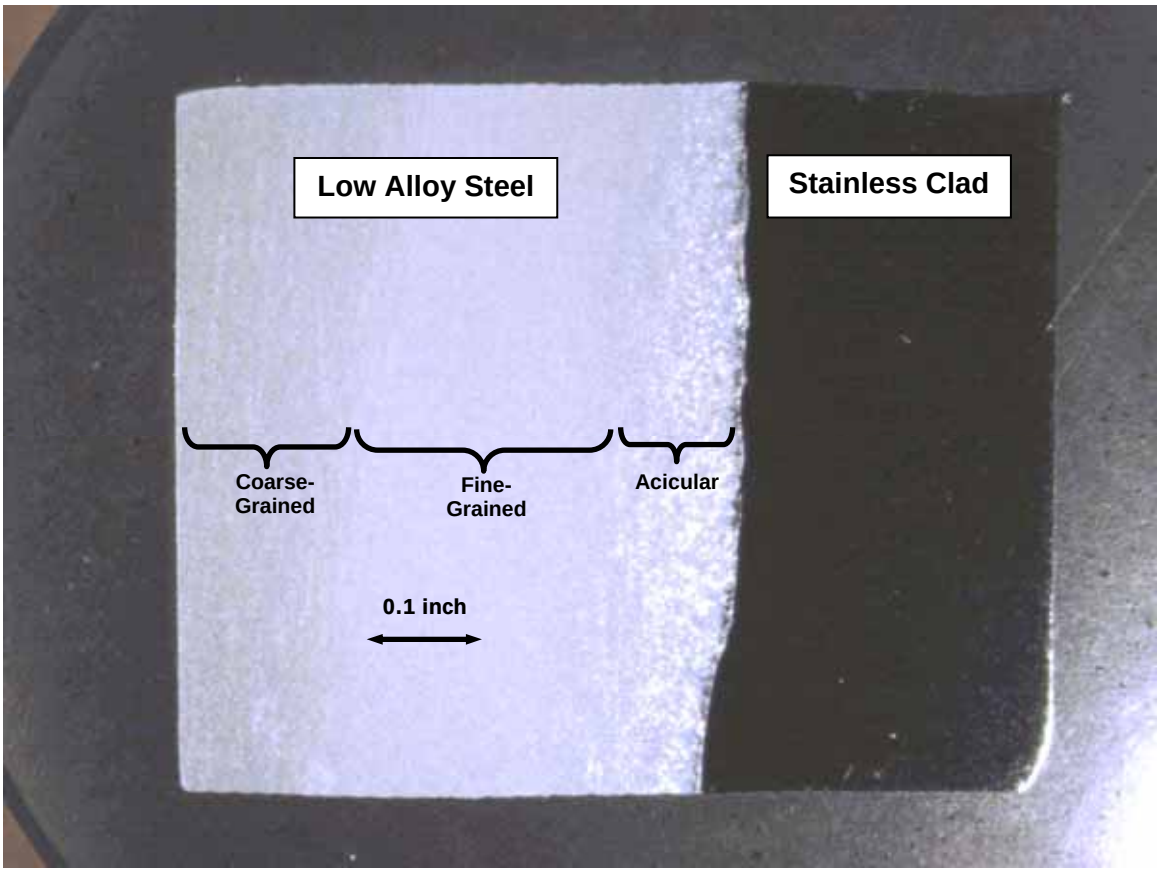

6X

Figure 4.2.1: Macro photograph of Sample B2C2B3 showing the low alloy steel stainless steel interface and various grain structures within the low alloy steel HAZ.

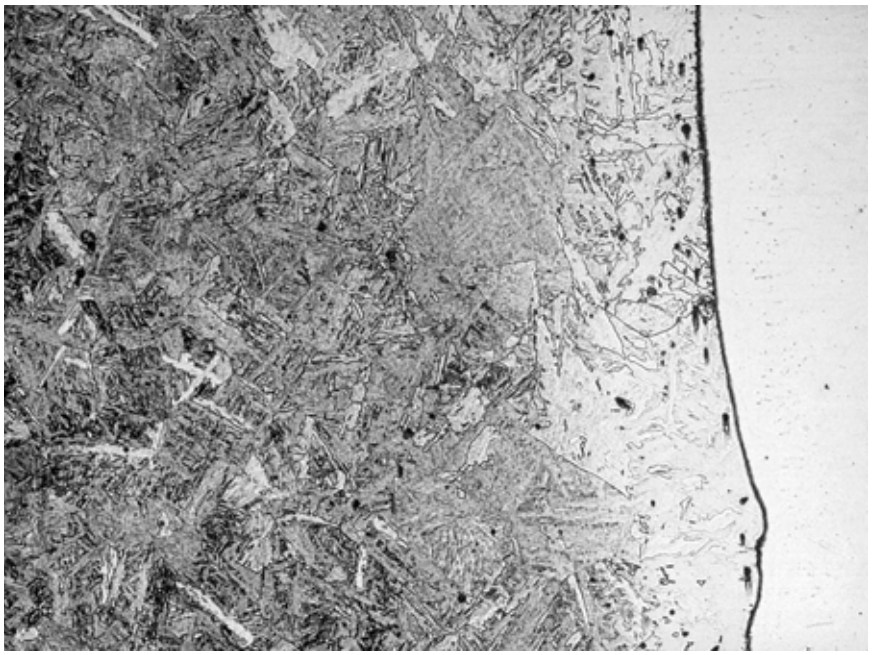

100X

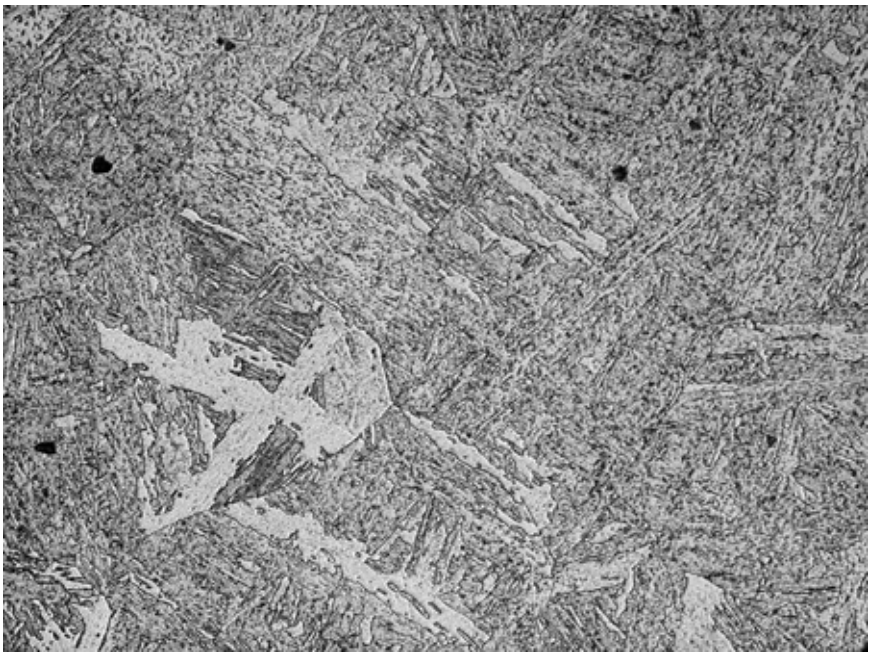

375X

Figure 4.2.2: Typical low alloy steel microstructures near bond. 2% nital

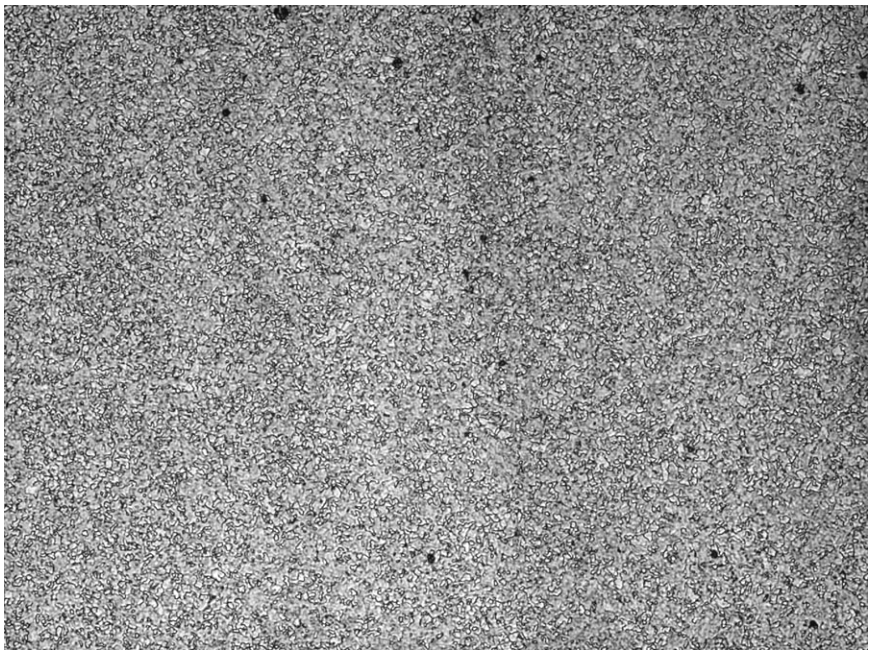

100X

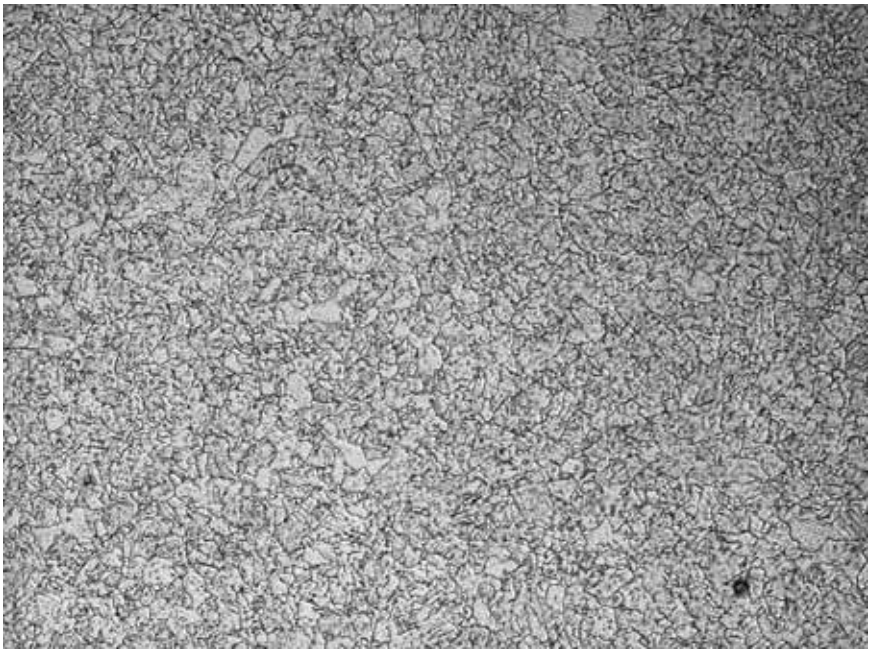

375X

Figure 4.2.3: Typical low alloy steel microstructures 1/4" from bond. 2% nital

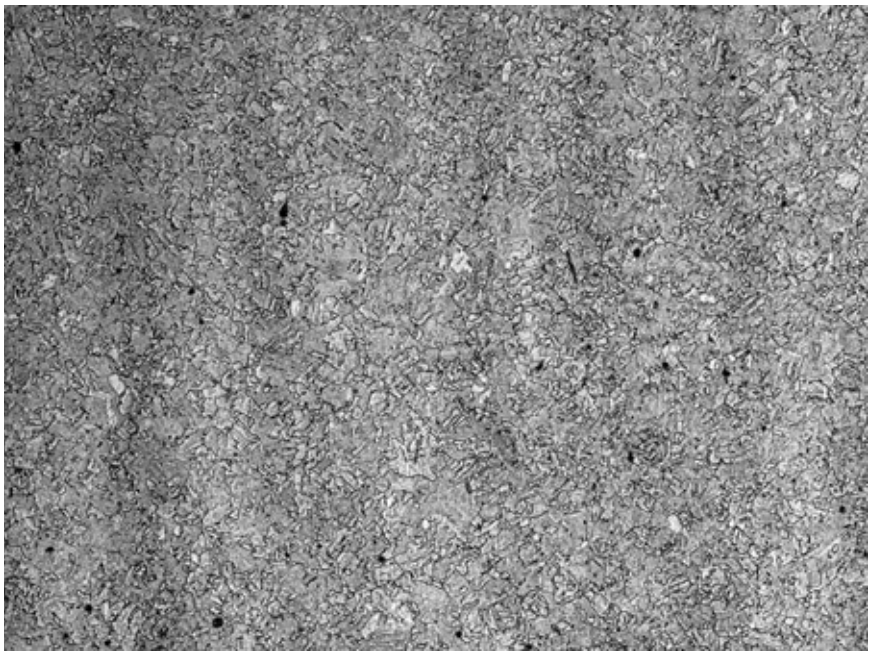

100X

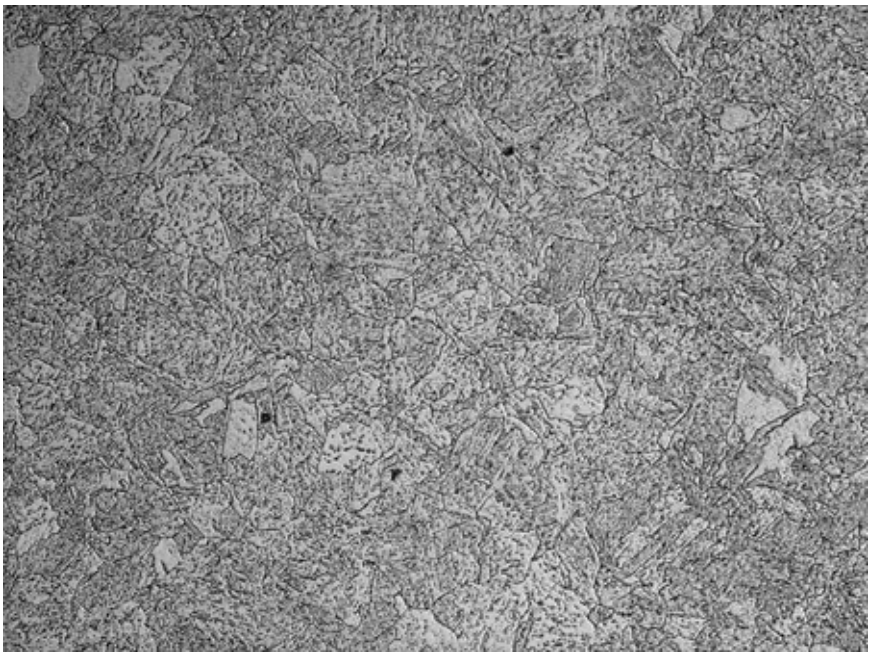

375X

Figure 4.2.4: Typical low alloy steel microstructures ~1/2" from bond. 2% nital

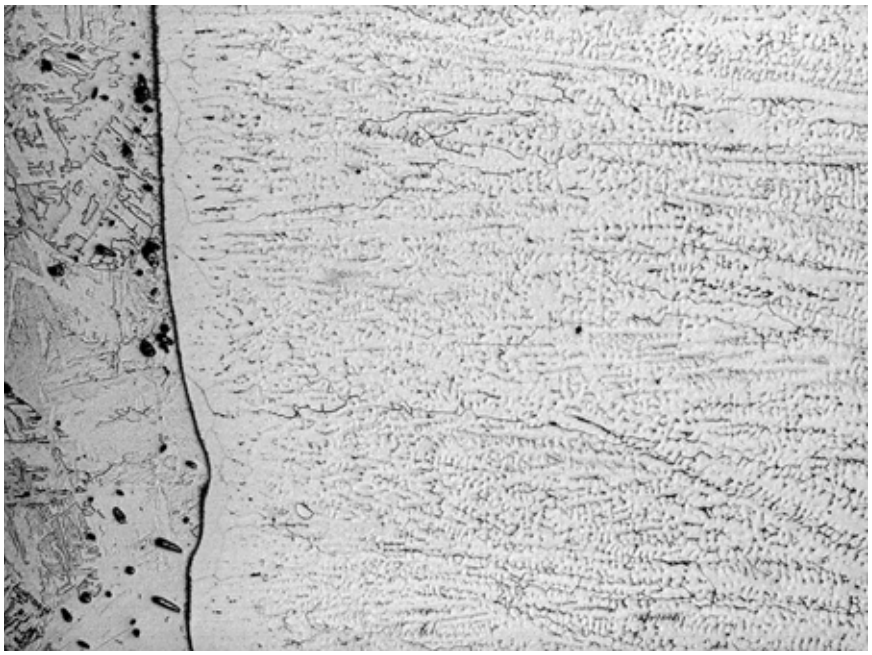

100X

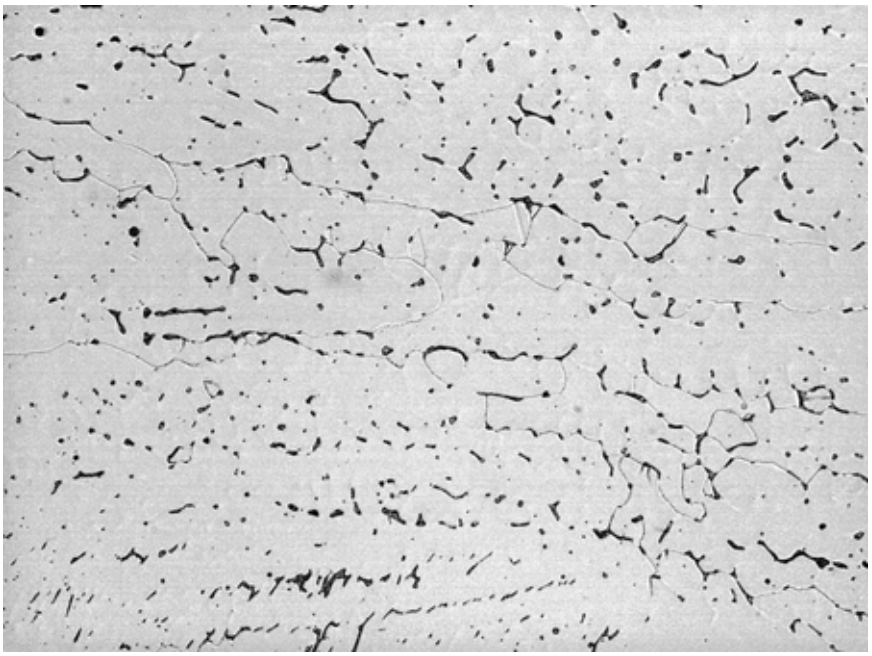

375X

Figure 4.2.5: Typical cladding microstructures near bond. (Acetic-nitric-hydrochloric etch)

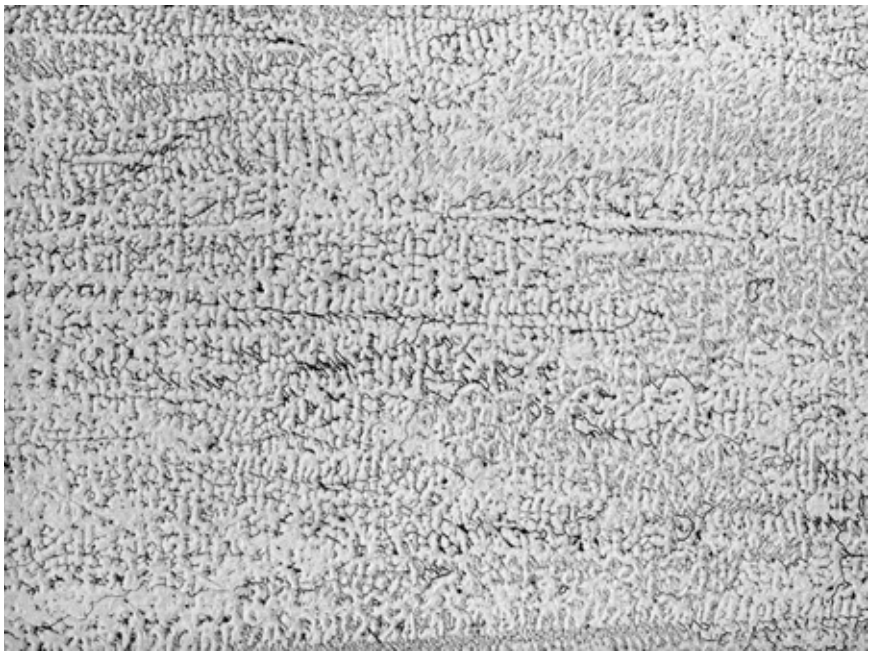

100X

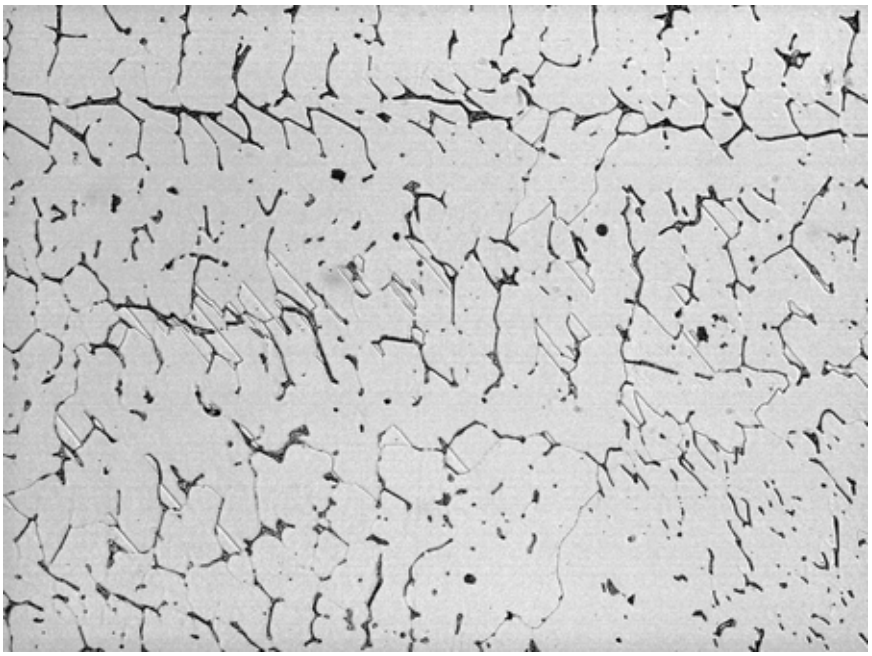

375X

Figure 4.2.6: Typical cladding microstructures away from bond. (Acetic-nitric-hydrochloric etch)